AALBORG UNIVERSITET Det Teknisk- Naturvidenskabelige Fakultet

Institute for Physics and Nanotechnology - Aalborg University

Silver Nanoparticles

P3 Project

Project Group N344

AALBORG UNIVERSITY
FACULTY OF PHYSICS AND NANOTECHNOLOGY

Skjernvej 4C ▪ DK-9220 Aalborg Øst

Title: Silver Nanoparticles
Project Period: 2^{nd} September 2005 - 9^{th} January 2006
Project Group: N344

Synopsis

This project is based on the initial problem: "How are the problems concerning the use of silver nanoparticles in industrial matters and commercial products to be handled". Silver nanoparticles exhibiting bactericidal properties are produced, and the production is described and discussed. The nanoparticles are produced by treating a solution of $AgNO_3$ dissolved in ethanol and PVP as solvent and stabilizer respectively with microwaves. The bactericidal effect of the synthesized particles is tested. A mathematical optical model describing the absorbance spectrum of silver nanoparticles is developed and compared to the absorbance data. The sizes of the produced nanoparticles are measured with DLS, SEM and AFM. The sizes are found to be between ~ 15 and $\sim 40nm$ in diameter and they show bactericidal effects. The conclusion to the project is that bactericidal nanoparticles have been produced. Furthermore is it concluded that the measuring methods does correspond to each other. DLS was found to be inappropriate for measuring the size of nanoparticles in presence of PVP. Finally it was found difficult to optimize the production in order to get homogenous particles, but it was found that one way to optimize the production was to change the ratio between PVP and silver nitrate.

Project group:
Nikolaj L. Kildeby
Ole Z. Andersen
Rasmus E. Røge
Tom Larsen
René Petersen
Jacob F. Riis

Supervisor:
Sergey I. Bozhevolnyi

Circulation: 9
Number Of Pages: 81
Finished: 20^{th} of December 2005

Preface

This report is the product of the P3 project period on Aalborg University - Faculty of Physics and Nanotechnology, and it has been published by group N344

The report is most of all directed to the supervisor and censor but also fellow students with a interest in this subject. A technical basis is therefore necessary to get a full understanding of the report.

Structure Of The Report

This report is build up by a main report followed by an appendix part. The main report consist of seven chapters; an introduction, a problem analysis, a method description, an optical model, the obtained results, a discussion of the results and finally a conclusion. The appendix part consist of different appendices, a thoroughly and technical description of the DLS technique and calculations used in the optical model. There will be references from the report to appendices where appropriate.

Instructions For Reading

It is expected that sections in each chapters are read together and the chapters are read in their chronological order.

The pdf version of the report, articles/webpages used in the report and data obtained from the various methods can be found on the enclosed cd-rom in the back of the report.

The notation used to references is the Harvard method and these are listed in alphabetic order in the bibliography, in the end of the main report.

Figures and tables are numbered sequentially in each chapter.

Thanks To

The authors would like to thank the following persons; Peter Fojan from Aalborg University for producing AFM pictures. The COM center at DTU for producing SEM pictures.

Contents

Chapter 1

Introduction

This chapter gives an introduction to the subject of nanoparticles and some of their unique properties. Some possible applications of silver nanoparticles will be described, and finally the project description and the initiating problem will be presented.

1.1 Why Nanoparticles?

One of the first and most natural questions to ask when starting to deal with nanoparticles is: "why are nanoparticles so interesting"?. Why even bother to work with these extremely small structures when handling and synthesis is much more complicated than that of their macroscopic counterparts. The answer lies in the nature of and unique properties possessed by nanostructures.

In our macroscopic everyday experience such phenomena as light act in an easily predictive way. Light directed at a surface is reflected just at the angle and with the color that would be expected. This easily predictive behavior changes dramatically when the reflecting particles become much smaller than the wavelength of the incident light.

Nanoparticles possess a very high surface to volume ratio. This can be utilized in areas where high surface areas are critical for success. This could for example be in the catalytic industry, some nanoparticles actually have proven to be good catalysts. Some nanoparticles also show bactericidal effects and here a high surface to volume ratio is also important.

In biology and biochemistry nanoparticles have attracted much attention. Nanoparticles are often in the range 10-100 nm and this is the size as that of human proteins. Scientists from the Chinese Academy of Science have even suggested using gold nanoparticles to improve Polymerase Chain Reaction (PCR).

In the production of anti-reflective optical coatings, nanoparticles have also proven valuable. Using metal oxides to coat polymeric films, anti-reflective surfaces have been created.

Nanoparticles does exhibit many interesting properties, and it is just a matter of time until more of these properties will be exploited. In the following sections a few of the possible uses of silver nanoparticles are described.

1.2 Applications of Silver Nanoparticles

Since the first nanoparticles were synthesized, their applications have found their way into many different areas of science. This section summarizes some of the most recent uses of silver nanoparticles.

1.2.1 Silver Nanoparticles as a Catalyst

A possible application of silver nanoparticles is the use as a catalyst. In the article *Catalytic Properties of Silver Nanoparticles Supported on Silica Spheres* [Jiang et al., 2004] this catalytic effect has been proven. This section is written using the results and conclusions of this article.

Silver nanoparticles immobilized on silica spheres have been tested for their ability to catalyze the reduction of dyes by sodium borohydride ($NaBH_4$). Catalysis of dyes was chosen because it is easy to detect a change in color when the dyes are reduced. In the absence of silver nanoparticles the sample was almost stationary showing very little or no reduction of the dyes. When silver nanoparticles were added to the solution, the sample rapidly. Figure 1.1 shows how the absorbance spectrum of the dyes decreases when the dyes are reduced. The reaction time showed to be strongly dependent on the concentration of silver nanoparticles. When the concentration was doubled, the reaction time was reduced to less than one third.

Silver nanoparticles act as an electron relay, aiding in the transfer of electrons from the BH_4^- ion to the dyes, and thereby causing a reduction of the dyes. BH_4^- ions are nucleophilic while dyes are electrophilic. It has been proven that nucleophilic ions can donate electrons to metal particles, while an electrophilic can capture electrons from metal particles. It has been shown that BH_4^- ions and dyes are simultaneously adsorbed on the surface of silver particles, when they were present together.

SEM pictures of the nanoparticles showed that they were intact after the reaction and still immobilized on the silica spheres. This proves that the particles acts as a catalyst because they are not consumed in the reaction, see Figure 1.1.

Silver nanoparticles have a strong tendency to agglomerate. This reduces the surface to volume ratio and thereby the catalytic effect. Therefore a stabilizing agent is often used to prevent agglomeration. However, the agent

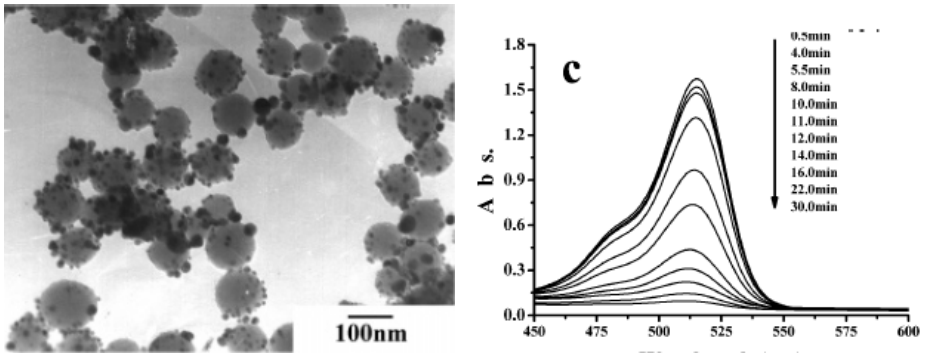

(a) Silica Spheres (b) Absorbance Spectra

Figure 1.1: (a) silver nanoparticles immobilized on silica spheres are illustrated. (b) The absorbance spectrum of the dyes decreases as the dyes are reduced by sodium borohydride. This process is catalyzed by silver nanoparticles. The arrow mark the increase of reaction time. Images from [Jiang et al., 2004]

is adsorbed on the surface of the nanoparticles, shielding them from the oxidant and reductant and thereby inhibiting the catalysis. Instead a new method for stabilizing the nanoparticles is used. The intermolecular forces which keep the nanoparticles immobilized on the silica spheres, has proven to be strong enough to prevent the particles from forming aggregates.

1.2.2 Silver Nanoparticles as a Bactericidal Agent

Another area where silver nanoparticles have proven to be effective is in controlling and suppressing bacterial growth. There have already been developed several applications which use the bactericidal effect of silver nanoparticles. This section will focus on results achieved in the article *Potential of Silver Nanoparticle-Coated Polyurethane Foam As an Antibacterial Water Filter* [Jain and Pradeep, 2004] which describes procedures to produce and test bactericidal foam.

The production of cheap and efficient water filters is necessary in order to clean infected water in undeveloped countries. These are the main target group as they are in desperate need of clean drinking water. The use of metal nanoparticles in water for disinfection is recent but experiments with metal ions and polymer films have been carried out for decades.

The purpose of the article was not to show that silver nanoparticles themselves have a bactericidal effect but instead to demonstrate the bactericidal effect of a silver nanoparticle-coated foam. Results from the coating process showed that silver nanoparticles was present in the foam after coating. They also showed to stay in the foam after washing with water. These

results showed that it was possible to coat PU foams with silver nanoparticles by a simple and cheap process.

Results from the tests, carried out on bacteria, showed that the coated foam had a bactericidal effect on E. coli. Three different tests was conducted in order to validate the result. The results from all three tests show that no bacteria was detected afterwards. The tests and results are in line with The World Health Organization (WHO, 1996) requirements for drinking water.

The overall result from the article clearly shows that the PU foams can be coated with silver nanoparticles and the bactericidal effect of these was validated. It also showed that silver nanoparticle coated foams can be used as water filters. As the chemicals used are cheap and commonly available and the coating process is simple, it should be possible to make this available to undeveloped nations.

1.2.3 Silver Nanoparticles as a Real-time Optical Sensor

Optical sensors of zeptomole (10^{-21}) sensitivity is another possible application using the potential of silver nanoparticles. Using the surface plasmon resonance effect the silver nanoparticles gain a very high sensitivity and the measurements can be conducted in real-time. This section is written using the results and conclusions of *Single Silver Nanoparticles as Real-Time Optical Sensors with Zeptomole Sensitivity* [McFarland and Duyne, 2003].

Silver nanoparticles show a peak in extinction, due to the localized surface plasmon resonance (LSPR) effect. More precisely this is caused by a collective excitation of the conduction band electrons of the nanoparticle. The λ_{max}-value of this plasmon resonance peak is dependent upon the size and shape as well as the solvent and adsorbates. The molar extinction coefficient is very high, ($3 \cdot 10^{11} M^{-1} cm^{-1}$) yielding a clear peak at even low concentrations.

Using the traditional uv-vis spectroscopy, the signal-to-noise ratio would make it impossible to detect the signal of a single nanoparticle even under the most optimal conditions. This can be avoided using Rayleigh scattering spectroscopy because this technique, though reducing the signal, minimizes the noise very effectively. This increases the sensitivity drastically as well as enables the detection of only a single nanoparticle. The experiments conducted in [McFarland and Duyne, 2003] showed that there is little difference between the sensitivity of a single silver nanoparticle and an array (sensitivities of 191 and 197 RIU^{-1} respectively).

The article showed results indicating a linear relationship of the LSPR λ_{max} with respect to the refractive index. The sensitivity (or proportionality coefficient) is dependent upon the shape and size of the nanoparticles. Furthermore the real-time response of the sensor was examined yielding a real-time response comparable with that of an array.

By controlling the size, shape and chemical modification of individual nanoparticles, an array of unique nanoparticles can simultaneously work as individual detectors. With the proper spacing between them an array of $50\mu m \times 50\mu m$ can be simultaneously screening for as many as 2500 different analysts.

One of the possible applications of the high sensitivity of the LSPR is for in vivo detection. It is possible to monitor the quantity of chemical species inside a cell as well as monitoring the dynamical processes that occur.

The time response tests yielded results comparable to that of other real-time response sensing technologies. The three principal visions of this technique is real-time optical sensing of a few molecules, massively parallel bio- and immunoassays and to form basis of in vivo sensing techniques.

1.3 Project Description

Today it is possible to synthesize metallic nanoparticles with many different shapes. Nanospheres, nanorods and nanocups are just a few of the shapes that have been grown. It is also possible to control the size of these particles to some extent. Using analytic techniques it is possible to determine the characteristics of the nanoparticles.

At this time, synthesis and characterization of nanoparticles is possible, but it is an expensive, time-consuming and not yet perfectly understood process. Before nanoparticles can be used commercially in fabrication of products available for the public, a number of issues have to be further examined. This report will focus on three main topics pertaining to silver nanoparticles.

A relatively easy way to synthesize silver nanoparticles by using a microwaves has been presented and used in numerous experiments. An investigation of this procedure will be the starting point for this project. In extension to this, characterization of the silver nanoparticles using a number of nanotechnological methods will be performed in order to achieve a knowledge of the size and shape of the nanoparticles. This will be compared to and discussed in relation to the synthesis method used.

The exceptional optical properties of silver nanoparticles will be investigated. Using optical theory on spherical particles smaller than the wavelength of light, a model for the optical spectrum of silver nanoparticles as a function of their size will be strived to be developed. This will be compared to empirical data from experiments.

Because silver has the ability to terminate bacterial division, and because nanoparticles has a very high surface to volume ratio, it is an obvious assumption that silver nanoparticles combines these two characteristics, thus

giving them remarkably bactericidal properties. This assumption will be investigated further as it might be a very interesting matter from a commercial point of view.

The subject of this report will be these three quite different topics, which is believed to be of great interest if the huge possibilities of silver nanoparticles are to be transferred into commercial products.

1.3.1 Initiating Problem

As pointed out in the project description the focus of this report will lie on the problems to overcome in order to use silver nanoparticles in commercial products. This leads up to the initiating problem:

- How are the problems concerning the use of silver nanoparticles in industrial matters and commercial products to be handled?

Chapter 2

Problem Analysis

Before an investigation of the optical properties and the bactericidal effects of silver nanoparticles can be examined and before applications are usable, it is crucial to be able to handle the synthesis in a satisfactory manner. A method for synthesizing nanoparticles using microwaves has already been mentioned in the introduction, and will be further described in later sections.

This chapter starts with a brief introduction to building nanostructures from the bottom, followed by a description of the crystal structures of nanoparticles. Next, the procedures and mechanisms concerning the synthesis of silver nanoparticles are described as well as the problems involved. After that, basic theories and experiences about the nature of light and about the bactericidal effect of silver nanoparticles is presented, before the problem analysis is concluded with project limitations and problem statement.

2.1 Top-Down vs. Bottom-Up

There are two approaches to the fabrication of metallic nanoparticles: top-down and bottom-up. The principle behind the top-down approach is to take a bulk piece of the material and then modify it into the wanted nanostructure. Cutting, grinding and etching are typical fabrication techniques, which have been developed to work on the nano scale [Britannica.com, 2005b]. The size of the nanostructures which can be produced with top-down techniques are between 10 to 100 nm.[Britannica.com, 2005b]

However, top-down has proven unsuccessful for several purposes. One of the problems with the top-down approach is the imperfection of the surface structure. Such defects in the surface structure can have a significant impact on physical properties and surface chemistry of the nanostructure due to the high surface to volume ratio. Even though there are problems connected to using a top-down approach, this is the method of choice when highly complex

structures are made. This is the case in the integrated circuit industry, where nanosized structures are cut in plain silica wafers using laser techniques. [Britannica.com, 2005b]

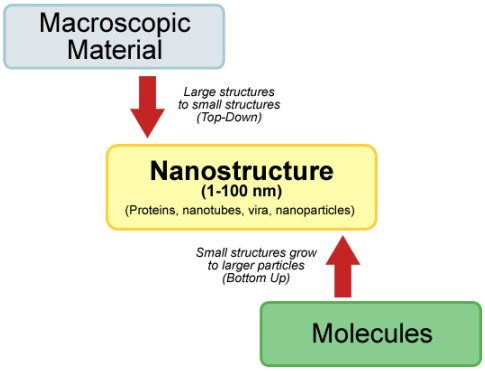

Figure 2.1: The top-down approach vs. the bottom-up approach.

Bottom-up, or self-assembly, refers to construction of a structure atom-by-atom, molecule-by-molecule or cluster-by-cluster. Colloidal dispersions used in the synthesis of nanoparticles is a good example of a bottom-up approach [Cao, 2004]. The size of the nanostructures, which can be obtained with a bottom-op approach, spans the full nano scale.

An advantage of the bottom-up approach is the better possibilities to obtain nanostructures with less defects and more homogeneous chemical compositions. This is due the mechanisms utilized in the synthesis of nanostructures reducing the Gibbs free energy, so that the produced nanostructures are in a state closer to a thermodynamic equilibrium. [Cao, 2004]

An illustration of the top-down approach vs. the bottom-up approach is shown in Figure 2.1

2.2 Crystal Structures

The crystal structure of nanoparticles is one of the main areas in which they differ from macroscopic particles. The ratio of surface atoms to interior atoms increase dramatically when the size of particles is in the nanometer scale compared with particles on larger scales, such as the micrometer scale. For example, for a cube of iron with an edge length of 1 cm the percentage of surface atoms is approximately $10^{-5}\%$. The percentage of surface atoms of an iron cube with an edge length of $10nm$ is in the order of 10% and when the edge length equals $1nm$ approximately all the atoms are surface atoms.

This increase in the ratio of surface atoms to interior atoms when dimensions are reduced to the nanometer scale, is one of the reasons why the synthesis of nanocrystals is so difficult to control. Due to the high percentage of surface atoms, nanocrystals possess a huge surface energy in relation

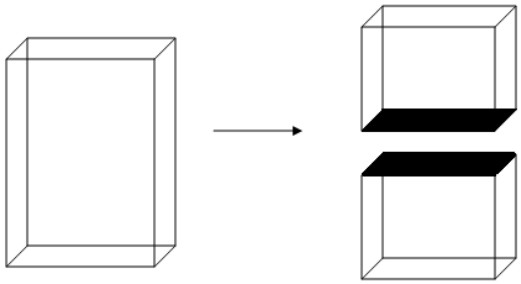

Figure 2.2: Shows how two new surfaces are created when a block is divided into two blocks.

to the total energy of the crystal. This surface energy makes nanocrystals thermodynamically unstable or metastable because it is no longer negligible in relation to the total energy of the crystal as it is in macroscopic crystals. Because of the significance of the surface energy it is important to understand what surface energy is and why crystals become thermodynamically unstable. [Cao, 2004]

The thermodynamically unstable state is caused by the fact that all atoms in a crystal attempts to reach the lowest possible energy. To minimize the total energy the atoms tries to avoid unsatisfied or dangling bonds. If there is no abnormality inside the crystal, all the dangling bonds will be localized on the surface of the crystal. Because of the dangling bonds, the atoms on the surface are under an inwardly directed force. This inward force decreases the bond distance between the surface atoms and the atoms in the sub-surface compared to the bond distance in the residual crystal. This decrease in bond distance between the surface atoms and the sub-surface atoms do not have any effect on a macroscopic crystal, but it can change the lattice constant of the entire crystal if the size of the particle is in the nanometer range. [Cao, 2004]

The extra energy caused by the dangling bonds in the surface atoms is normally referred to as the surface energy, surface free energy or surface tension. This energy is defined as the energy required to create a unit area of "new" surface.

A regular block divided into two blocks as illustrated in Figure 2.2 is considered. On the newly created surface, each atom is placed in an asymmetric environment because of the broken bonds. All the surface atoms are now exposed to an inward force, which pulls them toward the sub-surface. This inward force will rearrange the new surface atoms compared to their original position and create a new ideal surface. The energy which is required to get the surface atoms back to their original positions is the surface energy. An approximation of the surface energy is given by Equation 2.1.

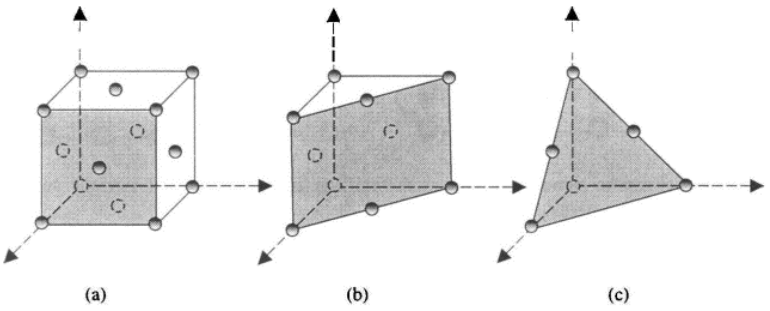

Figure 2.3: shows low index facets of a FCC crystal structure: (a){100}*, (b)*{110} *and (c)* {111}*. [Cao, 2004]*

$$\gamma = \frac{1}{2} N_b \varepsilon p_a \tag{2.1}$$

γ is the surface energy, N_b is the broken bonds per atom, ε is the bond strength and p_a is number of atoms per unit area on surface. This approximation only gives a rough estimation of the true surface energy. In a true calculation of the surface energy it is necessary to include interactions to higher order neighbor atoms and entropic or pressure-volume contributions. In spite of the approximation Equation 2.1 still gives some guidance of the true surface energy. [Cao, 2004]

Consider a silver crystal, which is a face-centered cubic (FCC) with a lattice constant a. Each silver atom has 12 neighbor atoms or its coordination number is 12. Each atom on a {100} facet will have four broken chemical bonds and the surface energy of a {100} facet will be:

$$\gamma_{\{100\}} = \frac{1}{2}\frac{2}{a^2} \cdot 4 \cdot \varepsilon = \frac{4\varepsilon}{a^2} \tag{2.2}$$

By comparison the surface energies of {110} and {111} facets are:

$$\gamma_{\{110\}} = \frac{5}{2}\sqrt{2}\frac{\varepsilon}{a^2} \approx 3,54\frac{\varepsilon}{a^2} \tag{2.3}$$

$$\gamma_{\{111\}} = 2\sqrt{3} \cdot \frac{\varepsilon}{a^2} \approx 3,46\frac{\varepsilon}{a^2} \tag{2.4}$$

The atoms in {110} and {111} facets have respectively 5 and 3 broken chemical bonds. The {100}, {110} and {111} facets can be seen in Figure 2.3.

From the calculations is it clear that a {111} surface gives the lowest surface energy followed by {110} and {100} surfaces. In general low indexes gives low surface energies and this is also the reason why stabile crystals are surrounded by low index surfaces.

This tendency to minimize the surface energy means that a synthesis of silver nanoparticles probably will result in nanoparticles with low index facets. [Cao, 2004]

2.3 Synthesis of Silver Nanoparticles

In extension to the general sections on the bottom-up method and the crystal structures, a more specific description of the formation of silver nanoparticles is presented.

In this project synthesis of silver nanoparticles is done using a bottom-up approach. Using a bottom-up approach gives the opportunity to produce silver nanoparticles between 1 and 10 nm. Bottom-up also gives the advantage of producing stable silver nanoparticles compared to silver nanoparticles produced with a top-down approach, because the nanoparticles are placed in defined crystalline structures. The stability of the nanoparticles is important when their properties are to be examined and exploited.

To understand the synthesis of silver nanoparticles the following sections will describe how silver nanoparticles are formed and how the growth can be controlled.

2.3.1 Reduction

The synthesis of silver nanoparticles in this project will be based on a wet-chemical method. The starting point of the synthesis is the production of a silver nitrate ($AgNO_3$) solution. When silver nitrate is dissolved it splits into a positive silver ion (Ag^+) and a negative nitrate ion (NO_3^-). In order to turn the silver ions into solid silver, the ions have to be reduced by receiving an electron from a donator. A flowchart illustrating the reduction of the silver ions by addition of an electron can be seen in Equation 2.5. The flowcharts of Equation 2.6 illustrates the reduction of (Ag^+) in a solution of ethanol. After the silver germ has been formed it starts to grow and continue the growth until the equilibrium between the final nanoparticles and the (Ag^+)of the solution is reached. [Chou et al., 2005]

$$Ag^+_{(aq)} + e^- \rightarrow Ag_{(s)} \tag{2.5}$$

$$2Ag^+_{(aq)} + C_2H_5OH + H_2O \rightarrow 2Ag_{(s)} + C_2H_50^-_2 + 3H^+ \tag{2.6}$$

There are a number of parameters that can be adjusted in order to control the growth of particles. For example, small particles can be achieved by using a fast reduction agent. A fast reduction agent results in the formation of many silver germs in the beginning of the synthesis process. This high amount of silver germs will abbreviate the time in which the germs can grow

and prevent the formation of large nanoparticles. If the solution is homogenous the particles end up within a narrow size distribution.[Cao, 2004]

Further control of the synthesis of silver nanoparticles can be obtained with the use of a stabilizer, which will be the topic of the next section.

2.3.2 Stabilizers and Solvents

A stabilizer is a substrate, often a polymer, with the purpose of preventing particles from agglomerating. This is done by producing a protective shell around the forming particle. The stabilizer is attached to the particle at one end of the polymer chain, making the polymer look like tentacles on the particle.

The efficiency of a certain stabilizer is connected with the properties of the solvent. If the solvent permits the stabilizer to stretch away from the particle the solvent is good. On the other hand if the solvent makes the stabilizer collapse on the surface of the particle the solvent is poor. This is only a problem if the particle is not covered 100% by stabilizer.

To explain this behavior it is necessary to look at the interactions between two 100% covered particles, which are dissolved in a good solvent. See Figure 2.4 for an illustration. When the two particles approach each other an interaction between them will first occur when the distance (d) between the particles becomes shorter than twice the thickness (L) of the polymer layer on the particles. This interaction between the two particles will increase the Gibbs free energy and they will repel each other. If there is not enough stabilizer present to cover the surface more than for instance 50% the polymers are inclined to interpenetrate in order to reduce the unoccupied space between polymers. As a result of such an interaction the freedom of the polymers decrease. This reduces the entropy of the system and results in an increase in Gibbs free energy, as it is illustrated in Figure 2.4.

An expression for the change in Gibbs free energy can be seen in Equation 2.7. ΔG is the change in Gibbs free energy, ΔH is the change in enthalpy, T is the temperature and ΔS is the change in entropy.

$$\Delta G = \Delta H - T\Delta S > 0 \tag{2.7}$$

A definition of ΔH is shown in Equation 2.8 where U_{sys} is the energy of the system, P is the pressure and V is the volume.

$$\Delta H = U_{sys} + PV \tag{2.8}$$

If the change in energy for the system of the two particles traveling towards each other approaches zero then ΔH can be said to be approaching zero. If this is taken into consideration while evaluating Equation 2.7 the

result is that the two particles covered with stabilizer repel on another. The distance between them must be $\geq 2L$. [Cao, 2004]

Figure 2.4 shows the interaction between two layers of polymer and the Gibbs energy as a function of distance.

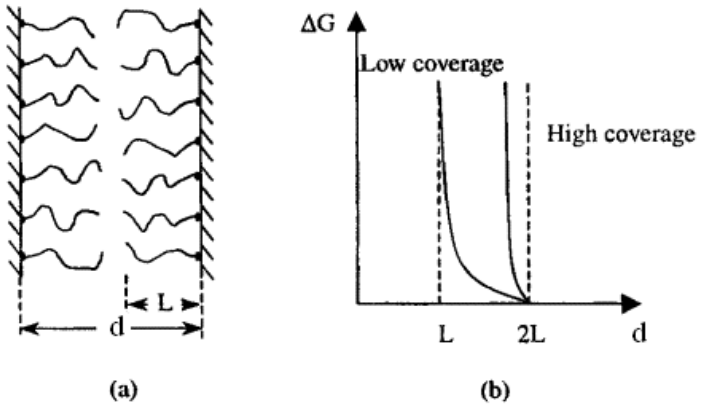

Figure 2.4: (a) two layers of polymers approaching each other (b) Gibbs free energy as a function of the distance between the two particles. modified from [Cao, 2004]

If the solvent is poor the polymers will coil together and collapse on the surface of the particle. This is not a problem when the nanoparticles are 100% covered by polymer. If the particle is not covered 100% and two particles move towards each other the result will be a decrease in Gibbs energy. This means that the polymers on the surface of one particle will interpenetrate with the polymers of the other and promote a further coiling. This in turn results in the two particles bundling together.[Cao, 2004]

When discussing good and poor solvents the important property to look at is the polar or nonpolar properties of the solvent. The polymers used as stabilizers have nonpolar properties which means that they are hydrophobic. If particles covered with these polymers are placed in a polar solvent such as water the polymers will pack together on the surface in order to minimize the contact surface where polymer meets water. To make the polymer expand away from the particle a nonpolar environment is needed. This could for example be methanol, ethanol or ethylenglycol. The solvent can also be categorized by its protic or aprotic properties. Protic solvents has the ability to exchange protons. The three solvents mentioned before are protic solvents. Benzene is an example of an aprotic solvent. [Cao, 2004]

In the synthesis of silver nanoparticles the stabilizer poly-vinyl pyrrolidone (PVP) has shown to be effective. PVP is a polymer made from the monomer N-vinyl pyrrolidone. Studies of the interaction between PVP and the forming silver particle with FTIR shows that in the case of particles

with diameters below 50 nm the nitrogen atom of PVP interacts with silver and forms a protective shell [Wang et al., 2005]. The complex formation between PVP and silver is described in Figure 2.5

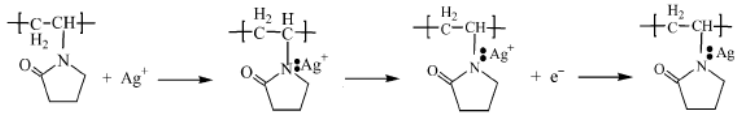

Figure 2.5: The complex formation between PVP and silver [Wang et al., 2005]

The use of a good solvent and an effective stabilizer does not only prevent the silver nanoparticles from agglomerating, it also shields the silver nanoparticles from the solution. This shielding stops the growth of the silver nanoparticles, which is a disadvantage when larger nanoparticles are wanted. Heating the solution is one way to solve this problem and an appropriate way to do this will be described in the next section. [Cao, 2004]

2.3.3 The Microwave Oven Method

The purpose of heating is to supply the reduced silver ions with enough kinetic energy to penetrate the polymer layer. This can be attained when the solution is heated in a microwave oven.[Cao, 2004]

Heating in a microwave oven is preferred over more conventional methods of heating, because it provides a uniform heat transfer to the solution. If the solution was heated on a heating plate, the local temperature at the interface between the solution, the bottle and the heating plate could easily reach temperatures much higher than the average temperature of the solution, causing an uneven heat transfer. An even heat transfer is critical for the formation of homogenous silver nanoparticles. A high temperature gradient through the solution could yield a wide size distribution of nanoparticles.

The diameter of the nanoparticles is crucial for their bactericidal effect. In general, only particles of sizes below 10 nm show the wanted bactericidal effect [Morones et al., 2005]. This is why it is necessary to tune the synthesis to particles of 10 nm in size.[Cao, 2004]

To sum up, the essential problems when synthesizing silver nanoparticles lies in controlling the processes and preventing the solid particles from growing to inappropriate sizes, or from bundling together and precipitate from the solution. Therefore control factors such as stabilizers are needed in order to grow a homogeneous size distribution of silver nanoparticles.

2.4 Tools for developing an optical model

In order to develop an optical model for light propagating in metallic nanoparticles, it is useful first to consider light propagating in free space, dielectrics and metals in a more general view. The wavefunctions become much more complex when working with specific cases, as for example silver nanospheres. In this section the basic steps for the later optical model will be taken.

2.4.1 Maxwell's equations

The nature of light has been a subject of investigation for several generations of physicists. The list of scientists working to reveal the nature of light contain names as Euclid (280B.C.), Pierre de Fermat (1601-1665), Christian Huygen (1629-1695) and Isaac Newton (1642-1727). It was however not until James Clerk Maxwell (1831-1879), with basis in various laws of electric and magnetic fields formed the equations now known as Maxwells equations, that an understanding of the phenomenon was achieved. [Klein and Furtak, 1986]

In 1861-1862 Maxwell developed his theory, stating that light is electromagnetic waves. By describing electric and magnetic fields and their inter-relation he derived the equations now known as Maxwell's equations. This is based on the assumption that light behaves like an electromagnetic wave. [Klein and Furtak, 1986]

This is a difficult theory to comprehend and in the beginning it had a mechanical analogy in ether being the medium in which the electric and magnetic fields propagated. It was imagined that the electric field was a distortion of charged ether particles and similarly the magnetic field was associated with rotating regions of ether particles. This concept of the ether, though aiding in understanding the theory, does not describe the real physical nature of light and has later been abandoned.

Experiments have repeatedly confirmed Maxwell's equations and the theory that light behaves as an electromagnetic wave. An important property to notice about Maxwell's equations is the fact that they are based on experiments and are therefore empirical formulas. The equations cannot be derived or proven in any theoretical way.

Today Maxwell's equations are the starting point from which all classical electromagnetic effects are explained. An example of the use of these equations is in determining the differential equation light must satisfy at the interface between ethanol and a silver nanoparticle.

Maxwell's four equations for light propagating in a medium of permittivity ϵ and permeability μ are given by Equation 2.9 to Equation 2.12. [Klein and Furtak, 1986]

$$\nabla \cdot \mathbf{D} = \rho \tag{2.9}$$

$$\nabla \cdot \mathbf{B} = 0 \tag{2.10}$$

$$\nabla \times \mathbf{E} = -\frac{\partial \mathbf{B}}{\partial t} \tag{2.11}$$

$$\nabla \times \mathbf{H} = \mathbf{J} + \frac{\partial \mathbf{D}}{\partial t} \tag{2.12}$$

ρ is the charge density, $\mathbf{E}$ is the electric field, $\mathbf{B}$ is the magnetic field, $\mathbf{H}$ is the magnetic intensity field, $\mathbf{D}$ is the electric displacement field, and $\mathbf{J}$ is the total current density. Furthermore two constants will be introduced in connection with these fields, the dielectric constant, ϵ_m given by the (electric permittivity)/(permittivity of free space) ratio, and the magnetic permeability, μ.

In general the dielectric constant and the magnetic permeability are dependent on the intensity of the field applied. However for most materials they can be approximated to be linear with good precision. This yields the definition of the electric displacement and magnetic intensity field given by Equation 2.13.

$$\begin{aligned} \mathbf{B} &= \mu \mathbf{H} \\ \mathbf{D} &= \epsilon_m \epsilon_0 \mathbf{E} \\ \mathbf{D} &= \epsilon_0 \mathbf{E} + \mathbf{P} \end{aligned} \tag{2.13}$$

$\mathbf{P}$ is the polarization vector. For light propagating in a dielectric, the charge density is zero, and Equation 2.9 equals zero. Furthermore there is no current and the total current density in Equation 2.12 also equals zero.

From Equation 2.11 the curl of both sides is taken and Equation 2.12 is inserted in Equation 2.11. Furthermore from the definition of the triple vector identity and Equation 2.9 the left side can be simplified. The definitions of the various fields from Equation 2.13 are used when needed.

$$\begin{aligned} \nabla \times \nabla \times \mathbf{E} &= -\nabla \times \frac{\partial \mathbf{B}}{\partial t} \\ \nabla(\nabla \cdot \mathbf{E}) - \nabla \cdot \nabla \mathbf{E} &= -\frac{\partial (\nabla \times \mu \mathbf{H})}{\partial t} \\ -\nabla^2 \mathbf{E} &= -\mu \frac{\partial^2 \mathbf{D}}{\partial t^2} \\ \nabla^2 \mathbf{E} - \mu\epsilon \frac{\partial^2 \mathbf{E}}{\partial t^2} &= 0 \end{aligned} \tag{2.14}$$

Equation 2.14 is a differential equation and the general solution is a periodic function in time and space such as the general waveequation. It should be noted that the same procedure can be repeated for the magnetic field and a similar differential equation would be obtained.

2.4.2 The wave equation

A solution to Equation 2.14 is given in Equation 2.15 which is the equation of the electric field of a wave propagating along the z-axis.

$$\mathbf{E}(z,t) = \mathbf{E}_0 \exp(i(\mathbf{k} \cdot z - \omega t + \phi)) \tag{2.15}$$

$\mathbf{k}$ is the wave vector, ω is the angular frequency, t is the time, and ϕ is a constant describing the phase of the light. From this equation it is evident that when freezing time you move along the wave in direction of propagation and when freezing the position, the amplitude of the electric field varies in time.

By applying the operators ∇ and $\frac{\partial}{\partial t}$ to the waveequation, it is clear that the space-time differentials can be replaced by the $i\mathbf{k}$ and $-i\omega$ respectively. This means that Equation 2.16 can be used when taking the space or time derivatives of a waveequation. Equation 2.16 is often referred to as the operator shortcuts.

$$\begin{aligned} \frac{\partial}{\partial t} &\rightarrow -i\omega \\ \nabla &\rightarrow i\mathbf{k} \end{aligned} \tag{2.16}$$

Using the operator shortcuts of Equation 2.14 the dispersion relation for k can be derived.

$$k^2 = \frac{4\pi^2}{\lambda^2} = \mu\epsilon\omega^2 = \frac{\mu\epsilon}{\mu_0\epsilon_0}\omega^2\mu_0\epsilon_0 = \frac{n^2\omega^2}{c^2} \tag{2.17}$$

n is the refractive index and is given by $\sqrt{\epsilon\epsilon_0^{-1}}$. $\mu_0\epsilon_0 = c^{-2}$ where c is the speed of light in vacuum. From the definition of μ_0 and ϵ_0 it is evident that the unit of c is meters per second. The speed of light and the fact that it is equal to $(\mu_0\epsilon_0)^{-1/2}$ was known prior to Maxwell but his theory gave the theoretical background. For electromagnetic waves traveling in a medium of a dielectric constant, ϵ_m and permeability, μ, the speed is given by $(\epsilon_m\epsilon_0\mu)^{(-1/2)}$.

By applying the operator shortcuts to Equation 2.11 the connection between the magnetic and electric field is illuminated.

$$-i\mathbf{k} \times \mathbf{E} = -i\omega\mathbf{B}$$

yielding

$$\mathbf{B} = \omega\mathbf{k} \times \mathbf{E} \tag{2.18}$$

This proves that the electric field and the magnetic field must both be perpendicular to the direction of propagation as well as perpendicular to each other. From Equation 2.18 it is clear that the electric and magnetic field are in phase with each other.

2.4.3 Optical properties of metals

When electromagnetic waves radiate on the surface of a conducting medium an electric field is applied. This field will result in a force acting on the free electrons of the metal, which is showed in Figure 2.6.

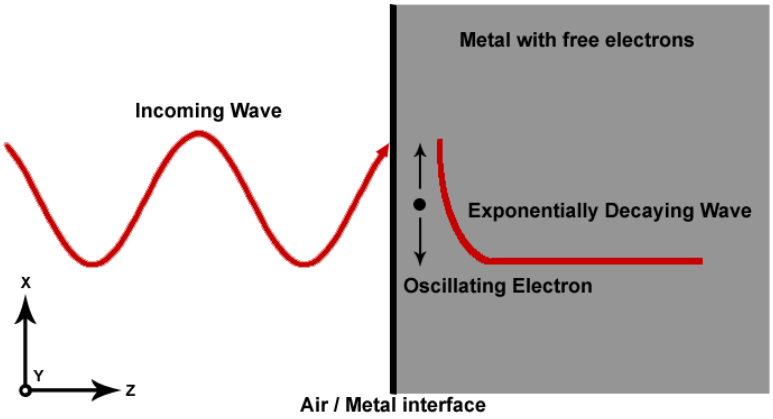

Figure 2.6: When electromagnetic waves propagates into a metal an electric field is applied causing the electron to experience an electric force. As the wave cannot propagate into the metal the field attenuates exponentially

The only forces acting on the electron is the electric field and a dampening force. If the fields were applied to the electron in free space, then there would be no dampening but as the electron in a metal will collide frequently the dampning factor is necessary. The dampening factor is experimentally determined.

The direction of the propagating light is set as the z-axis, and as illustrated in Figure 2.6 the motion of the electron as well as the electric field is described by the x-axis. When Newtons 2^{nd} law is applied to the motion of the electron, Equation 2.19 yields.

$$m\frac{\partial^2 x}{\partial t^2} = -m\Gamma\frac{\partial x}{\partial t} - e\mathbf{E} \tag{2.19}$$

e is the charge of the electron, Γ is the dampning factor, m is the mass of the electron and $\mathbf{E}$ is the electric field applied by the incoming electromagnetic radiation.[Klein and Furtak, 1986]

The oscillating electric field and movement of the electron can be described by a time independent factor times the time dependent part.

$$\mathbf{E}(x,t) = \mathbf{E}_0(x)\exp(-i\omega t) \quad \text{and} \quad x(t) = x_0\exp(-i\omega t) \tag{2.20}$$

From Equation 2.20, Equation 2.19, and the operator shortcuts of Equation 2.16 the expression for x in Equation 2.21 is derived.

$$\begin{aligned} -m\omega^2 x &= m\Gamma i\omega x - e\mathbf{E} \\ x &= \frac{\frac{e}{m\omega^2}}{(1+\frac{\Gamma}{\omega}i)}\mathbf{E} \end{aligned} \tag{2.21}$$

The electric dipole moment for a unit volume of electrons displaced in the direction of x is given by Equation 2.22.

$$\mathbf{P} = -Nex \tag{2.22}$$

N is the number of electrons in a unit volume of the metal. Equation 2.21 is inserted in Equation 2.22 yielding Equation 2.23.

$$\mathbf{P} = -\frac{\frac{ne^2}{m\omega^2}}{(1-\frac{\Gamma}{\omega}i)}\mathbf{E} \tag{2.23}$$

in which the plasma frequency is defined by Equation 2.24. This factor is only dependent of the metal. A model for the crystal and electron structure is needed for a complete description of the optical features.

$$\omega_P = \frac{Ne^2}{m\epsilon_0} \tag{2.24}$$

From a description of the electric displacement field an expression for the dielectric constant is found. The dielectric constant is given by $\epsilon_m = \epsilon\epsilon_0^{-1} = n^2$.

$$\begin{aligned} \epsilon_m(\omega) &= 1 + \frac{\mathbf{P}}{\epsilon_0\mathbf{E}} \\ \epsilon_m(\omega) &= 1 - \frac{\omega_p^2}{\omega(\omega+\Gamma i)} \end{aligned} \tag{2.25}$$

From the definition of the wavevector in Equation 2.17 it is evident that the wavevector becomes complex for light propagating in metals. The wavevector is separated into the real and the imaginary part.

$$\tilde{\epsilon_m} = \epsilon_{m,Re} + i\epsilon_{m,Im} = 1 - \frac{\omega_p^2}{\omega^2+\Gamma^2} + \frac{\omega_p^2\Gamma}{\omega(\omega^2+\Gamma^2)}i \tag{2.26}$$

From evaluating the general expression for a plane wave with the now complex wavevector, Equation 2.27 is easily derived.

$$\mathbf{E} = E_0 \exp(-\epsilon_{m,Im}\frac{\omega^2}{c^2}z)\exp(i(kz-\omega t+\phi)) \tag{2.27}$$

The wave now attenuates exponentially with the factor $\exp(-\epsilon_{m,Im}\frac{\omega^2}{c^2}z)$.This is also illustrated in Figure 2.6.

2.4.4 Localized Surface Plasmon Resonance

Optical properties of metallic nanoparticles are dependent on the their dimension. This section will describe the size dependence of the localized surface plasmon resonance (LSPR) for metallic nanoparticles.

LSPR is an in-phase oscillation of electrons lead by the coherent excitations of all free electrons in the conduction band. A LSPR is generated when the size of a metallic nanocrystal is smaller than the wavelength of incident radiation. A simple illustration of the surface plasmon oscillation is shown in Figure 2.7. The LSPR is a dipolar excitation between the negatively charged electrons and the positive charge lattice in the particle. [Cao, 2004]

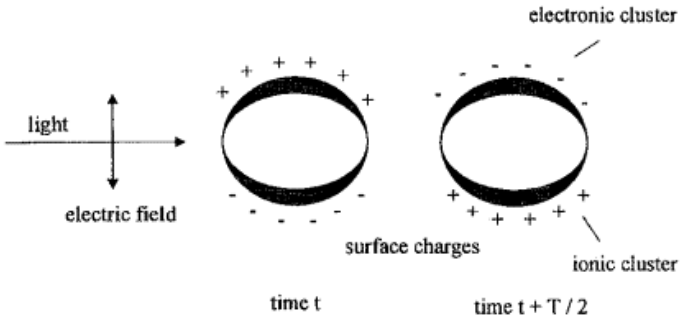

Figure 2.7: The electric field of the incoming light wave induces a polarization of the free electrons relative to the cationic lattice. The net charge difference is only induced at the surface of the spherical metallic nanoparticle. This acts as an restoring force, causing a dipolar oscillation of the electrons with a period T. [Cao, 2004]

It has been shown by Gustav Mie in 1908 that the LSPR depends explicitly on the particle size. This can be seen in the absorption spectra where both the absorbtion wavelength and peak increases as the particle size increases. However, this is only valid for larger nanoparticles. In a small particle where the mean free path of the conducting electrons is smaller than the physical dimension of the nanoparticle, the electron surface scattering becomes significant. For silver nanoparticles the limit is $20nm$. The smaller the particle, the faster the electrons reach the surface and the scattering loses the coherence faster. As a result, the plasmon bandwidth increases when particle size decreases. [Cao, 2004]

2.5 Detection of Silver Nanoparticles

An essential issue in this project is the experimental detection and investigation of silver nanoparticles. The first step is to determine whether silver nanoparticles are actually synthesized or not. In addition characterization of the nanoparticles to examine size, shape, and quantity is important. A number of different measurement techniques can be used for this purpose, including Atomic Force Microscopy (AFM), Scanning Electron Microscopy (SEM), Absorbance Spectroscopy and Dynamic Light Scattering (DLS). A brief introduction to these techniques is presented here.

2.5.1 Absorbance Spectroscopy

Absorbance spectroscopy is used to determine the optical properties of a solution. Light is send through the sample and the amount of absorbed light is measured. When the wavelength is varied and the absorbance is measured at each wavelength, a *(wavelength, absorbance)* graph can be drawn using computer software.

The applications of absorbance spectroscopy are extensive. For example, the absorbance can be used to measure the concentration of a solution by using *Beer-Lamberts Law*.

However, for examination of nanoparticles, the optical properties are much more complicated and require an individually developed theory. For instance, the measured absorbance spectrum does not necessarily show the actual absorbance but the extinction of the light. The extinction is both the absorbed and the scattered light from the particles. The theory will not be further discussed in this section but will be illuminated in the following sections, and eventually derived in Chapter 4.

2.5.2 Dynamic Light Scattering

The DLS technique uses light to determine the size of particles in a solution. Light at a given frequency is sent through the solution from a laser. When the light interacts with the moving particles in the solution and is scattered, the frequency of the light is also changed. This change of light frequency is directly related to the size of the particles in the solution; the smaller the particles, the greater the shift in the light frequency. This difference in the light shift is used to determine the size of the particles in the solution.

DLS is capable of measuring particles in the size range from a few nanometers to a few micrometers. It is therefore applicable for determining the size of silver nanoparticles. A more detailed description of DLS is described in Appendix A.

2.5.3 Scanning Electron Microscope

When high-resolution images of the surface of a sample is desired, the SEM is a valuable instrument. The microscope works by the same principle as an optical microscope, but instead of photons it measures the electrons scattered from the sample. Because electrons can be accelerated by an electric potential, the wavelength can be made shorter than the one of photons. This makes the SEM capable of magnifying images up to 200.000 times. At the same time it is possible to achieve high resolution pictures of the surface, making the instrument very useful in determining the size distribution of nanoparticles.

2.5.4 Atomic Force Microscope

The AFM is an instrument capable of measuring the topography of a given sample. A nanosized tip attached on a cantilever is traced over the sample and a 3D image of the sample topography is generated on a computer.

The advantage of the AFM over SEM is the ability to make topographical measurements for detection and investigation of the size and shape of silver nanoparticles in three dimensions. Thus, the AFM makes it possible to determine the height of the particles.

2.6 The Bactericidal Effect of Silver Nanoparticles.

The growth of unwanted bacteria has for a long time been and is still a problem for the food industry and in the medical field. Therefore, there is a need for methods to kill or slow down the growth of unwanted bacteria. An interesting alternative to existing methods is the use of metallic nanoparticles, which exhibit bactericidal properties. One of the most promising types of metallic nanoparticles is silver nanoparticles.

In order to achieve an understanding of this effect, knowledge about the structure of bacteria is needed. In particular, the bacterial membrane and the contained proteins are of special interest, because the silver has to react with it in order to penetrate the bacteria.

2.6.1 Bacteria

Bacteria are unicellular microscopic organisms which consists of one compartment containing all the elements of the cell, including DNA. They are in overall divided in two main groups; gram positive and gram negative, which refers to two different types of membranes. The gram positive bacteria have a thick mesh-like shell consisting of peptidoglycan, that protects the single

bilayer phospholipid membrane. The gram negative have a thin layer of peptidoglycan enclosed by two bilayers of phospholipid. [Britannica.com, 2005a]

In order for the bacteria to interact with the surroundings they have integrated proteins in the membrane. Each of these proteins has a specific use. Some are so-called ion channels that allows ions to move in or out of the cell by diffusion. Others are proteins that transport molecules by consumption of energy in the form of ATP.

Furthermore there is a third type of membrane proteins consisting of three subtypes. The first of these is the so called uniporters where an already thermodynamically favorable reaction is enhanced by allowing molecules to migrate through a membrane from high concentration towards low. This means that the uniporters actually allow a substance that cannot penetrate the phospholipid membranes by diffusion, to enter the cell using the catalyzing properties of the protein. The last two of the three is the so called cotransporters which work by using the energy of a thermodynamical favorable migration of substrate such a ions to catalyze the transport of another substrate against its concentration gradient. [Lodish et al., 2000]

2.6.2 The microbiological effect of silver ions

Silver has for a long time been known to be toxic to a wide range of bacteria, and this has been utilized in various applications. Silver compounds are used as preservatives in a variety of products and in the medical field to treat burns and infections. The bactericidal effect of silver can be divided into two groups; the reactive component being either silver ions or silver nanoparticles. Here a clear distinction between ions and particles has to be made. To clarify, silver ions are charged atoms (Ag^+) whereas silver nanoparticles are single crystals of nanosize dimensions.

In spite of the fact that the bactericidal effect of silver ions is well known and used it is still not fully understood. Experiments have shown that silver ions are able to make structural changes in the cell membrane. The membrane of bacteria contains of lot of sulfate-containing enzymes and it has been proposed that silver ions interact with these sulfate-groups and thereby change the membrane morphology by pacifying the enzymes. This inactivation makes the membrane vulnerable and easier to penetrate for silver ions. Inside the cell, silver ions continue to destroy different parts of the cell by interacting with sulfate-groups, which are often located in the active site of enzymes. This interaction with the active site causes an inactivates of the enzymes.

Silver ions are also able to interact with phosphorus-groups of molecules and experiments have shown that this can have severe effects. One example is the interaction between silver ions and the backbone of DNA, which makes the bacteria unable to replicate itself or transcribe mRNA for new proteins. All these changes slow down the growth of the bacteria and finally kills it.

However, the bactericidal mechanism of silver nanoparticles on bacteria is almost unknown. It has been proposed that the effect is caused by some of the same mechanisms that causes the bactericidal effect of silver ions. [Alcamo, 1997]

2.6.3 Bacteriological experiments testing the effect of silver nanoparticles

A series of experiments have been performed to test the bactericidal effect of silver nanoparticles. Four different gram negative bacteria, P. Aeruginosa, V. Cholera, S. Typhus and E. Coli, have been treated with silver nanoparticles of different size and shape. [Morones et al., 2005]

The conclusions of the experiments are that silver nanoparticles interact with the surfaces as well as the interior of the bacteria. Figure 2.8 shows that silver nanoparticles interact with the membrane and the interior of an E.Coli bacteria. These interactions between silver nanoparticles and the bacteria look quite similar to the interactions between silver ions and bacteria. This may indicate that the silver nanoparticles are able to interact with the same types of chemical groups as silver ions and are thereby able to cause the same types of damages to the bacteria as silver ions are.

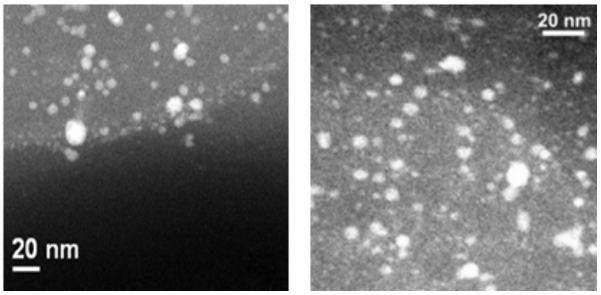

(a) (b)

Figure 2.8: The effect of silver nanoparticles in the membrane and the inside of E.Coli. The pictures are taken with a STEM [Morones et al., 2005]. (a) The E. coli membrane, where the presence of silver nanoparticles is observed. (b) The interior of the E. coli. Again, the presence of silver nanoparticles is observed.

2.6.4 The mechanism of the bactericidal effect of Silver Nanoparticles

The silver nanoparticles which show interaction with the bacteria were all between 1 and 10 nm. The reason for this size dependency is probably a combination of the particles' ability to react with and penetrate the cell

membrane and the higher surface to volume ratio of smaller particles. It is known that small ($\sim 5nm$) metallic particles present electronic effects, which are defined as changes in the local electronic structure of the surface. These effects enhance the reactivity of the nanoparticle surfaces. When the size of the silver nanoparticles decreases the percentage of the interacting atoms increases, and this could be the explanation to why small ($1-10nm$) silver nanoparticles are able to interact with the bacteria. With regard to the ability of silver nanoparticles to penetrate the cell membrane, is it reasonable to believe that small nanoparticles are more capable of penetrating the cell membrane than large nanoparticles. [Morones et al., 2005]

The morphology of the interacting silver nanoparticles have also been studied, and the majority of the silver nanoparticles were either octahedral, multiple-twinned icosahedral or decahedral in shape. In common for these types of particles is the high amount of {111} facets. Previous experiments have demonstrated that {111} facets exhibit high reactivity, which may explain why these types of particles are capable of interacting with bacteria. See Figure 2.3 for an illustration of {111} facets.

When silver nanoparticles are present in a solution they secrete a small amount of silver ions, which will have an additional contribution to the bactericidal effect of silver nanoparticles.

No articles describing the study of transport of silver nanoparticles via membrane proteins has been found, but it has been proven that the nanoparticles enter the cell. This indicates that they interact with the membrane proteins; but it has however not been proven. Also, the experiments shows that silver nanoparticles indeed exhibit bactericidal properties and that the bactericidal effect depends strongly upon the size and shape of the nanoparticles. [Morones et al., 2005]

2.7 Health effects of Silver Nanoparticles

Silver nanoparticles have been proposed as an antibiotic and as a preservative, and this means that the particles will come in close contact to human beings. This makes it important to study the effect that silver nanoparticles might have on human health. Compared to other properties of silver nanoparticles there have been only little research in the effects of silver nanoparticles on health. It is well known that metals in general change properties as the size approaches the nano scale. In regard to this, and the fact that silver nanoparticles possess bactericidal properties, the health effects on human beings is an area which has to be thoroughly examined. In humans digestion is dependent on bacteria and it would be fatal if silver nanoparticles could interfere with and kill these bacteria. This section will examine the different aspects regarding the health issues of silver nanoparticles.

The article *In Vitro Cytotoxicity of Nanoparticles in Mammalian Germline Stem Cells* is one of the few articles which describes the effect of silver nanoparticles on germ cells [Braydich-Stolle et al., 2005]. If the germline is affected negatively it could cause a mutation or other genetic change in the germline and this might have an negative effect on the offspring. The article is a study with the purpose of evaluating the suitability of a mouse spermatogonial stem cell line as a model to evaluate the toxicity of nanoparticles in male germline in vitro. Different nanoparticles (silver, molybdenum and aluminium) was tested in regard to cell morphology, mitochondrial function and membrane leakage.

The cell morphology was tested to see if nanoparticles had an impact. The test showed that silver nanoparticles changed the morphology drastically and this change caused apoptosis, cell death, to some cells.

The mitochondrial function and viability of the germline stem cells was tested in order to see if the nanoparticles had an effect on these. It showed that silver nanoparticles reduced mitochondrial function and viability drastically even at low concentrations, between 5 and 10 μg/ml.

Membrane leakage was tested to see if the nanoparticles had any effect on this. The results showed that silver nanoparticles only cause a slight increase in the membrane leakage, indicating that silver particles interfere with cell metabolism instead of the plasma membrane. Interfering with cell metabolism could promote cell apotosis and this was confirmed by the cell morphology test. [Braydich-Stolle et al., 2005]

The overall result showed that silver nanoparticles did interfere with germline stem cells and that they were the most toxic nanoparticle used in these studies.

A different aspect in the research of the health effect of silver nanoparticles comes from Odense Universitets Hospital i.a. According to their research, silver is piled up in the body but there has been no evidence of intoxication or side effects due to this. It furthermore shows that silver nanoparticles should be released from the body with time [ouh.dk, 2005]. Other companies such as Samsung supports this statement as they claim to have tested their products in regard to health effects [samsung.com, 2005].

It seems impossible to conclude whether silver nanoparticles entail a health hazard or are harmless to human beings. But there are no doubt that nanoparticles may cause unpleasant effects because of their size and properties. The size makes them highly mobile in the environment as well as in the human body. They can enter human tissue through lungs, skin and digestion and this could cause health problems. This tells that it is necessary to perform more scientific studies before it is ethically justifiable to release any nanoparticle-product. If nanoparticle-products are sent to the market before testing, and they show to be toxic, it could scare people away from other nano-products in the future.

2.8 Project Limitations

The main approach to this project is to examine the bactericidal effect of silver nanoparticles and in this respect it is necessary to use nanoparticles in the size of 10 nm. Escherichia coli (E.Coli) is one of the most applied bacteria in laboratories because it is fast growing, easy to control and normally non-toxic. Therefore it will also be used in this project for bacteriological experiments. Furthermore there are two other approaches to the project, the synthesis of silver nanoparticles and the derivation of a mathematical optical model to describe their absorbance spectrum.

In order to control the size of the particles a production method described in an article from 2002 is used. This article describes the production of silver nanoparticles with ethanol as solvent and PVP as stabilizer [Frattini et al., 2005]. There are several other ways to synthesize silver nanoparticles. To other examples can be seen in [Chou et al., 2005] and [Grijalva et al., 2005] but they will not be described any further. Only the methods used in the project is described.

To further assist in controlling the size of the nanoparticles it will be useful to relate the color of the solvent to the size of the nanoparticles. An optical model will therefore be made in order to optically examine the size of the nanoparticles. Absorbance Spectroscopy will be used in order to validate the optical model and the size of the particles will be measured using DLS, AFM and SEM.

To sum up, this project will focus on testing the bactericidal effect of silver nanoparticles, production of nanoparticles optimal for inhibiting bacterial growth, and finally a simple optical model to describe the size of nanoparticles from the color of the solution.

2.9 Problem Statement

This project has two main purposes. The primary purpose is to produce silver nanoparticles “small enough” to cause the death of bacteria. The second purpose is to make an optical model for the behavior of nanoparticles when they are exposed to light. Furthermore, the following questions will be answered.

- How does the bactericidal effect depend on the size of the silver nanoparticles?
- How does the size measuring methods correspond to each other?
- How can the synthesizing methods be optimized to give the desired size distribution.

Chapter 3

Materials & Methods

This chapter describes the procedures used for synthesizing silver nanoparticles and testing their bactericidal effect. The first section describes how the synthesis is carried out, the next section describes the characterization of the synthesized nanoparticles and the last sections are dedicated to describing the procedures for testing the bactericidal effect. In the appropriate sections all experimental parameters (chemicals, amounts, times etc.) are shown.

3.1 Synthesis of Silver Nanoparticles

This and the following sections serves the purpose of describing the process of synthesizing silver nanoparticles according to the theory described in Section 2.3. Table 3.1 shows information on the chemicals used for synthesis.

Name	Formula	CAS#	Conc.
Polyvinylpyrrolidone	$(C_6H_9NO)_n$	9003-39-8	-
Silver Nitrate	$AgNO_3$	7761-88-8	99.5%
Ethanol	C_2H_5OH	64-17-5	96%

Table 3.1: The chemicals used for synthesis of silver nanoparticles. PVP with a molecular weight of 40,000 g/mole is used.

3.1.1 Synthesis of Silver Nanoparticles in an Ethanol Solution

PVP (40,000 g/mole) and ethanol is poured into a 100 mL pyrex flask. The solution is mixed by a magnetic stirrer until PVP is dissolved. Silver nitrate

is added to the solution and stirring continues until the silver nitrate is dissolved. All solutions are made by dissolving $1.0g$ of PVP and either $0.1g$ (low concentration, $0.25g/100mL$) or $0.5g$ (high concentration, $1.25g/100mL$) of silver nitrate in $40mL$ EtOH. Two different concentrations of silver nitrate are tested to determine if the amount of silver ions in the solution has an impact on particle formation. All the samples and their synthesis parameters are listed in Table 3.2.

Sample	P [W]	Time [min]	Conc. of $AgNO_3$	Rest. b/a
1a	160	2	High	$\sim 15min$/-
1b	160	5	High	$\sim 15min$/-
1c	160	7	High	$\sim 15min$/-
1d	160	10	High	$\sim 15min$/-
1e	160	20	High	$\sim 15min$/-
2a	160	2	Low	$\sim 15min$/-
2b	160	5	Low	$\sim 15min$/-
2c	160	7	Low	$\sim 15min$/-
2d	160	10	Low	$\sim 15min$/-
2e	160	20	Low	$\sim 15min$/-
3a	160	20	Low	$\sim 15min$/-
3b	160	20	Low	$\sim 1month$/-
4a	750	0.5	High	-/$\sim 24h$
4b	750	0.5	Low	-/$\sim 24h$

Table 3.2: P is the microwave effect measured in Watts. Time is the microwave exposure time measured in minutes. Conc. of $AgNO_3$ is either low (0.25g/100mL) or high (1.25g/100mL). Rest. time shows how many minutes the solution rested before/after microwave treatment before analyzed. 1a through 1e are made at high concentration with the microwave treatment time varying. 2a through 2e are made at low concentration with the time varying. 3a and 3b are made at low concentration and treated at 160 watt for 20 minutes. 3b is allowed to rest for 1 month after microwave treatment before being analyzed. 4a and 4b are are mixed and allowed to rest for 24 hours before being treated for 30 seconds at 750 watt. 4a is at high concentration and 4b is at low concentration.

The solutions are heated in a microwave oven for variable exposure times. In most of the samples the microwave effect is set to 160 watt to avoid extensive boiling of the solution. Even at 160 watt continuous heating of the solution causes boiling and bumping of the solution, and therefore the solution is heated discontinuously. The solution is first brought to its boil-

ing point and thence allowed to cool until heating can be continued. This procedure is continued until the solution has been exposed to microwave irradiation for the decided period of time. $0.5mL$ is removed from the stock solution and heating of the residual stock solution is continued until the next period of time has elapsed. $0.5mL$ is again removed from the stock solution and heating of the stock solution continues again. This process continues until solutions of all the decided irradiation periods has been retrieved.

Two samples are prepared at 750 watt 24 hours after mixing. These samples are made and analyzed to test if the effect of the microwaves has an impact on particle formation.

3.2 Characterizing Synthesized Particles

The synthesized particles are analyzed by absorbance spectroscopy, DLS, SEM and AFM. This section describes how the analyses are made.

3.2.1 Analysis by Absorbance Spectroscopy

Before recording the absorbance spectrum a reference of pure 96% EtOH is recorded. Because the optical density of the sample itself is too high for recording the spectrum at an acceptable noise level, the sample is diluted 1:12. The spectrophotometer used is a S2000 and the software used is Ocean Optics OOIBase32 Version 2.0.2.2.

3.2.2 Analysis by Dynamic Light Scattering

The cuvette is washed in 96% EtOH and allowed to dry. The sample is poured into the cuvette and placed in the instrument. The computer software is set to take account of the refractive index, viscosity, and temperature coefficient of EtOH. The analysis will show the average radius size of the particles in the solutions. The instrument used is a ProteinSolution Dynapro 99 and the software used is DYNAMICS Version 5.

3.2.3 Analysis by Scanning Electron Microscopy

Silicon wafers are used to support the sample when the silver nanoparticles are examined in the SEM. To get a smooth coating of the silicon wafers they are spin coated at 1500 RPM for 15 secs. $30\mu L$ of sample is put on the wafer before spin coating. The prepared wafers are shielded from dust while the ethanol vaporizes, and then examined in the SEM. The instrument used is a LEO 1550 SEM.

3.2.4 Analysis by Atomic Force Microscopy

As with SEM, the samples are prepared on silicon wafers by spin coating at 1500 RPM for 15 secs. A major difference between SEM and AFM is that the PVP layer on the wafer is not seen in SEM. In AFM however, the PVP layer is seen and it is likely to dominate the picture so the nanoparticles are not detected. Therefore the wafers are flushed with ethanol immediately after spin coating. This clears away most of the PVP layer. The instrument used is a Multimode^{TM} Atomic Force Microscope and the software used for evaluation of the data is NanoScope Version 5.12.

3.3 Testing the Bactericidal Effect of Silver Nanoparticles

The production of LB plates for growth of E. Coli bacteria is firstly described. After that the actual methods for testing the bactericidal effect are described. Several methods are tried out to find the one best suited for testing the bactericidal effect. Three independent lines of experiments are carried out. The first line tests which method is best suited to detect if nanoparticles kill bacteria. Using this method, the next line tests which areal density $[Ag/m^2]$ of the synthesized nanoparticles is optimal to kill bacteria. This experiment is made to prevent using more silver than necessary.

The last line, using the best method and the optimal dilution found, tests which silver nanoparticles synthesizing procedure yields the best bactericidal effect. Here it is important to use the dilution found in the last experiment line. If a too high concentration is used, the silver will kill all bacteria independently on the size of the particles.

3.3.1 Production of LB Medium and LB Plates

To produce the LB plates, a solution of LB agar medium is firstly produced. In Table 3.3 the mixtures and the amount of each mixture is shown.

The LB medium is autoclaved for 20 minutes at 121°C and then poured into petri dishes. The dishes are allowed to cool to room temperature to solidify the LB medium, and put in a refrigerator for later use.

3.3.2 Propagation of Bacteria

The bacteria are frozen at -80°C when received. They are put into ice water and allowed to unfreeze slowly.

One LB plate and 8 mL liquid LB medium is used for propagation of bacteria. The bacteria is inoculated onto the plate and incubated at 37°C over night. The bacteria E. Coli strain B(21CDE3) is used. When the

Compound	Amount	CAS#
MilliQ Water	400 mL	-
Bacti Casein Peptone	4.0 g	91079-38-8
Yeast Extract	4.0 g	8013-01-2
Sodium Chloride	2.0 g	7647-14-5
Agar	6.0 g	9002-18-0

Table 3.3: The compounds and the amount of each compound used to produce the LB medium. Agar is only added when producing LB medium to be used for plates. The liquid medium to be used for propagation of bacteria does not contain agar.

colonies appear, one colony is chosen and put into the 8 mL liquid LB medium. This solution is shake incubated at 150 RPM and 37°C for 3-4 hours.

Some of the LB plates are inoculated with a thin film of E. Coli. This is done by putting 500μL E. Coli LB medium onto an LB plate, and spreading the medium on the whole plate. The plates are incubated at 37°C for 24 hours afterwards.

3.4 Finding the Best Suited Treatment Method

Because the silver nanoparticle solution contains ethanol, the solution cannot be put directly onto an LB plate with bacteria. The ethanol would kill the bacteria immediately. This section describes various methods for testing the bactericidal effect.

3.4.1 Immobilization on a Glass Plate

A glass plate is treated with nanoparticle solution, and the ethanol is allowed to vaporize. With the side prepared with nanoparticles facing down, the glass plate is put onto an LB plate prepared with a thin film of E. Coli.

The glass plate prevents the bacteria underneath from "breathing", and if the bacteria are killed in the experiment it is unknown if this is caused by silver nanoparticles or asphyxiation. Therefore a reference E. Coli treated LB plate with a glass plate not treated with silver nanoparticles is made.

3.4.2 Immobilization on a Filter Paper

A non air-tight filter paper is prepared with a silver nanoparticle solution and the ethanol is allowed to vaporize. This leaves a filter paper with nanoparticles attached to it. This filter paper is placed on a LB plate prepared with a thin film of bacteria.

As with the glass plate approach, a reference E. Coli treated LB plate with an untreated filter paper is made. From this plate it can be seen if the filter paper itself kills the bacteria.

3.4.3 Direct Treatment of LB Plates

Direct treatment of an LB plate with the silver nanoparticles solution is the last method tried out. Half of an LB plate is treated with $100\mu L$ silver nanoparticles solution and the ethanol is allowed to vaporize. The other half of the petri dish is treated with $100\mu L$ E. Coli and this is inoculated from the one half into the silver nanoparticle treated half. This procedure is illustrated in Figure 3.1.

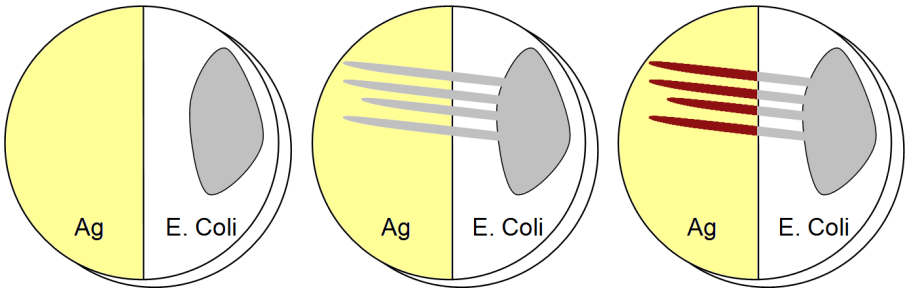

Figure 3.1: The procedure of testing by direct treatment of LB plates. (a) First silver nanoparticles are put on one half of a petri dish, and E. Coli on the other half. (b) E. Coli is inoculated from the E. Coli prepared half into the silver nanoparticles half. (c) After incubation at 37°C for 24 hours it is seen that the bacteria which crosses onto the silver nanoparticles prepared half are killed and no colonies are formed.

Using this procedure it can be clearly seen if silver nanoparticles kills the bacteria, because no colonies will form on the nanoparticle side if growth is inhibited by nanoparticles.

As with the two other approaches is a reference plate made. Half of the LB plate is treated with PVP before E. Coli is spread on the LB plate. This reference is made to see if the PVP kills bacteria.

3.5 Finding the Production Method Best Suited for Inhibiting Bacterial Growth

These experiments are made to find out which microwave treatment period of silver nanoparticle solution yields the best bacteria inhibiting silver

nanoparticles. It is expected that the different periods yield nanoparticles of different sizes, and it is known that $< 10nm$ nanoparticles exhibit the best bactericidal properties.

If the concentration of nanoparticles in the solution is high, the areal density of nanoparticles $[Ag/m^2]$ will be high too. This could cause death of bacteria independently on the size of the nanoparticles. Therefore, the samples are diluted before they are tested. Dilutions of 1/4, 1/8, 1/12, 1/16, 1/20, 1/26, 1/32, 1/64, 1/128 and 1/256 silver nanoparticle solution are made. The dilutions are tested and the dilution which kills bacteria, but still leaves some living colonies on the LB plate is used in further experiments.

To test the bactericidal effect of the different production methods, the method described in Section 3.4 which showed to be best for testing is used. The samples are diluted according to the results obtained from the dilution experiment and tested.

Chapter 4

Developing An Optical Model

$\mathbf{e^{i\pi} + 1 = 0}$

A fundamental part of this report is the absorbance spectra as they are the easiest and fastest way to obtain information on the solution of silver nanoparticles. However, the absorbance spectrum alone tells only little about the sample.

Through an optical model it is possible to determine a relationship between the size and shape of silver nanoparticles and the absorbance spectrum. The optical model is calculated for an approximated structure. In this report the subject is nanospheres of small radii.

The data referred to as the absorbance spectra of the experimental part of this report is in fact the extinction spectra. The extinction is the sum of the absorbance and scattering of the sample. Therefore the main goal of this chapter will be to derive an expression for the extinction cross section.

4.1 The Waveequations

In the path for the extinction cross section it is necessary to derive some introductory formula. As will be shown later the extinction cross section is dependent on the electric field inside the nanoparticle. Therefore the derivation of this will be the first goal.

The electric and magnetic fields must at all times suffice Maxwell's equations. These equations provide the linkage between the electric and magnetic fields of the incoming light as well as other conditions. From these equations the initial differential equation that light must suffice can be derived. The Maxwell equations describing this situation are given in Equation 4.1 to Equation 4.4.

$$\nabla \cdot \mathbf{D} = \rho \tag{4.1}$$
$$\nabla \cdot \mathbf{B} = 0 \tag{4.2}$$
$$\nabla \times \mathbf{E} = -\frac{\partial \mathbf{B}}{\partial t} \tag{4.3}$$
$$\nabla \times \mathbf{H} = \frac{\partial \mathbf{D}}{\partial t} \tag{4.4}$$

Silver is approximated as a linear medium enabling the use of Equation 2.13 and thereby simplifying the model significantly. Although no material is perfectly linear at the energies at which the model will be taken in use the flaw is very small.

The differential equation is derived in a way similar to that of Section 2.4, taking the curl on both sides of Equation 4.3 and combining with Equation 4.4.

$$\nabla \times \nabla \times \mathbf{E} = -\nabla \times \frac{\partial \mathbf{B}}{\partial t} = -\mu \frac{\partial (\nabla \times \mathbf{H})}{\partial t} = -\mu \frac{\partial^2 \mathbf{D}}{\partial t^2} = -\mu\epsilon \frac{\partial^2 \mathbf{E}}{\partial t^2}$$

The electric and magnetic field can be written as $\mathbf{E}(\mathbf{r}, t) = \mathbf{E^0}(\mathbf{r}) \exp(i\omega t)$. By keeping the time constant and allowing the field to vary only in space the following is derived.

$$\frac{\partial^2 \mathbf{E}}{\partial t^2} = \frac{\partial^2}{\partial t^2}(\mathbf{E^0}(\mathbf{r}) \exp(i\omega t)) = -\omega^2 \mathbf{E}^0(\mathbf{r}) \exp(i\omega t)$$

$$\mu\epsilon\omega^2 \mathbf{E}^0 - \nabla \times \nabla \times \mathbf{E}^0 = 0 \tag{4.5}$$

Equation 4.5 is the differential equation which the waves must suffice. From Mie theory it is given that the waves are defined to satisfy the Helmholtz equation.

$$(\nabla^2 + k^2) g(\vec{r}) = 0, r \neq 0 \tag{4.6}$$

The incoming and the scattered wave when frozen in time are given by Equation 4.7 and Equation 4.8.

$$\mathbf{E}^0_{inc} = \hat{z} E_0 \tag{4.7}$$
$$\mathbf{E}^0_{scat} = G \cdot \hat{z} \alpha E_0 \tag{4.8}$$

Where $g(r)$ and G are defined as

$$g(r) = \frac{\exp(-ikr)}{4\pi r}, r \neq 0 \tag{4.9}$$
$$G = (\frac{1}{k^2}(\nabla\nabla + k^2 I) g(r)) \tag{4.10}$$

The incoming and scattered waves are given in advance as it is a tedious work to derive them. This is a first approximation of the Mie scattering theory which will not be treated in this report. Therefore the starting point is the waveequations of Equation 4.8 and Equation 4.7 which must satisfy the differential equation Equation 4.5. For the incoming wave this is easily shown and focus will be given the scattered wave.

Using the triple vector product the left side of Equation 4.5 is changed.

$$-\nabla(\nabla \cdot \mathbf{E}_{scat}) + \nabla^2 \mathbf{E}_{scat} + k^2 \mathbf{E}_{scat} = 0 \tag{4.11}$$

The expression for the scattered wave of Equation 4.8 is inserted in Equation 4.11. Note that $g(r)$ is called g for short however it is still a function of r.

$$-\frac{1}{k^2}\nabla[(\nabla\nabla^2 + k^2\nabla)g]\hat{z}\alpha\mathbf{E}_0 + (\nabla^2 + k^2)[\frac{1}{k^2}(\nabla\nabla + k^2)g]\hat{z}\alpha\mathbf{E}_0 = 0 \tag{4.12}$$

This can be repositioned into Equation 4.13.

$$-\frac{1}{k^2}\nabla\nabla[(\nabla^2+k^2)g(r)]\hat{z}\alpha\mathbf{E}_0+\frac{1}{k^2}(\nabla\nabla+k^2 I)[(\nabla^2+k^2)g(r)]\hat{z}\alpha\mathbf{E}_0 = 0 \tag{4.13}$$

Both the terms in the brackets becomes zero when using the Helmholtz equation. The scattered wave is now proven to satisfy the differential equation of Equation 4.5.

4.2 Boundary Conditions

In order to satisfy the boundary conditions over the surface of the silver nanoparticle it is advantageous to use spherical coordinates. The expression for E_{inc} in spherical coordinates is given by Equation 4.14. See Appendix B.3 for definitions of spherical coordinates.

$$\mathbf{E}_{inc} = \hat{z}E_0 e^{-ikr} \approx \hat{z}E_0 = (\hat{r}\cos\theta - \hat{\theta}\sin\theta)E_0 \tag{4.14}$$

For E_{scat} it becomes more complicated. Firstly the Taylor series of $g(r)$ to the 3^{rd} term is used as an approximation. For small r a good approximation for the term $G \cdot g$ is expressed in Equation 4.15. This derivation is clarified in Appendix B.2.

$$G \approx \frac{1}{4\pi k^2 r^3}(-I + 3\hat{r}\hat{r}) - i\frac{k}{4\pi}I \tag{4.15}$$

Using this approximation for calculating E_{scat} for spherical coordinates Equation 4.16 yields. Note that r is replaced with a since it is the boundary conditions which is considered.

$$\begin{aligned} \mathbf{E}_{scat} &= G\hat{z}E_0 \\ \mathbf{E}_{scat} &\approx [\frac{\theta\sin\theta + 2\hat{r}\cos\theta}{4\pi k^2 a^3} - \frac{ik}{6\pi}(\hat{r}\cos\theta - \hat{\theta}\sin\theta)]\alpha E_0 \end{aligned} \tag{4.16}$$

The wave inside the sphere is defined in Equation 4.17.

$$\mathbf{E}_{sph} \approx \hat{z}E_{sph} = (\hat{r}cos\theta - \hat{\theta}\sin\theta)E_{sph} \tag{4.17}$$

In order to determine the boundary conditions on the surface of the silver nanoparticle the symmetry of the sphere can be used. At any point on the surface there is complete tangential symmetry. In spherical coordinates this ensues that continuity of the tangential and radial component is a sufficient condition.

Crossing the surface of the sphere there is a difference in the refractive index. Therefore the boundary conditions for the tangential component becomes:

$$n_m^2\hat{r}\cdot\mathbf{E}_{sph} = n_s^2\hat{r}\cdot(\mathbf{E}_{inc} + \mathbf{E}_{scat}) \tag{4.18}$$

Note that when calculating the dot product, $\mathbf{r}\cdot\mathbf{E}$, only the terms of $\mathbf{E}$ containing $\hat{r}$ will remain will remain as $\hat{\theta}$ is perpendicular to $\hat{r}$.

$$\begin{aligned} n_m^2\cos\theta E_{sph} &= n_s^2[\cos\theta + \frac{2\alpha}{4\pi k^2 a^3}\cos\theta - \frac{ik\alpha}{6\pi}\cos\theta]E_0 \\ E_{sph} &= \frac{n_s^2}{n_m^2}(1 + \frac{\alpha}{2\pi k^2 a^3} - \frac{ik}{6\pi})E_0 \end{aligned} \tag{4.19}$$

The tangential boundary condition using spherical coordinates is expressed in Equation 4.20.

$$\hat{\theta}\cdot\mathbf{E}_{sph} = \hat{\theta}\cdot(\mathbf{E}_{inc} + \mathbf{E}_{scat}) \tag{4.20}$$

Through insertion and simplification Equation 4.21 yields.

$$\begin{aligned} -\sin\theta E_{sph} &= (-\sin\theta + \frac{\alpha}{4\pi k^2 a^3}\sin\theta + \frac{ik\alpha}{4\pi k^2 a^3}\sin\theta)E_0 \\ -E_{sph} &= (-1 + \frac{\alpha}{4\pi k^2 a^3} + \frac{ik\alpha}{6\pi})E_0 \end{aligned} \tag{4.21}$$

Through addition of either side of Equation 4.19 to Equation 4.21 the term, E_{sph} can be eliminated. From a series of calculations α can be isolated.

$$\frac{n_s^2}{n_m^2}(1+\frac{2\alpha}{4\pi k^2a^3}-\frac{ik}{6\pi})E_0+(+\frac{\alpha}{4\pi k^2a^3}-\frac{ik\alpha}{6\pi}-1)E_0=0$$
$$\alpha[\frac{2n_s^2}{n_m^2}+1+4\pi k^2a^3(\frac{ik}{6\pi}-\frac{in_2^2k}{n_1^26\pi})]=4\pi k^2a^3(1-\frac{n_2^2}{n_1^2})$$
$$\alpha[2n_s^2+n_m^2+i4\pi k^2a^3(n_m^2-n_s^2)\frac{k}{6\pi}]=4\pi k^2a^3(n_m^2-n_s^2)$$
$$\alpha=4\pi k^2a^3\frac{(n_m^2-n_s^2)}{2n_s^2+n_m^2+i4\pi k^2a^3(n_m^2-n_s^2)\frac{k}{6\pi}} \tag{4.22}$$

Using the expression for α found in Equation 4.22, E_{sph} can be isolated.

$$\begin{aligned}
E_{sph} &= [1-4\pi k^2a^3\frac{(n_m^2-n_s^2)}{2n_s^2+n_m^2+i4\pi k^2a^3(n_m^2-n_s^2)\frac{k}{6\pi}}(\frac{1}{4\pi k^2a^3}+\frac{ik}{6\pi})]E_0\\
&= [1-\frac{(n_m^2-n_s^2)(1+i4\pi k^2a^3\frac{k}{6\pi})}{2n_s^2+n_m^2+i4\pi k^2a^3(n_m^2-n_s^2)\frac{k}{6\pi}}]E_0\\
&= [\frac{2n_s^2+n_m^2+i4\pi k^2a^3(n_m^2-n_s^2)\frac{k}{6\pi}+n_s^2-n_m^2-i4\pi k^2a^3(n_m^2-n_s^2)\frac{k}{6\pi}}{2n_s^2+n_m^2+i4\pi k^2a^3(n_m^2-n_s^2)\frac{k}{6\pi}}]E_0\\
&= [\frac{3n_s^2}{2n_s^2+n_m^2+i4\pi k^2a^3(n_m^2-n_s^2)\frac{k}{6\pi}}]E_0
\end{aligned} \tag{4.23}$$

One last modification is needed before the expression for the electric field inside the silver nanoparticle is applicable to finding the extinction cross section. In Equation 4.23 the denominator is complex, making it very tedious to complex conjugate the expression.

$$\mathbf{E}_{sph}=\mathbf{E}_0\frac{3\epsilon_s(\epsilon_m^*+2\epsilon_s-i4\pi k^3a^3(\epsilon_m^*-\epsilon_s)\frac{k}{6\pi})}{|2\epsilon_s+\epsilon_m|^2} \tag{4.24}$$

In order to reach the expression of Equation 4.24 it is necessary to cancel some terms in the denominator. These terms are, however, all containing a higher degree of r and for small r these terms will have little effect on the equation.

4.3 Finding the extinction cross section

The extinction cross section for a spherical silver nanoparticle can be calculated with Equation 4.25.

$$\sigma_{ext}=-\mathrm{Im}\{\frac{\mathrm{k_0}}{\mathrm{n_s}|\mathbf{E}_{\mathrm{inc}}|^2}\int_{\mathrm{V}}[\mathbf{E}_{\mathrm{inc}}(\mathbf{r})]^*\cdot(\mathrm{n_m^2}-\mathrm{n_s^2})\mathbf{E}_{\mathrm{sph}}\mathrm{dV}\} \tag{4.25}$$

k_0 is defined to be $\frac{\omega}{c}$. This expression is rather complex, therefore a simplification would be an advantage. The first step is to replace k_0 with k/ϵ_s. Subsequently $\mathbf{E}_{inc}$ can be substituted with $\mathbf{E}_0 \cdot \exp(-i\omega t)$ since the radius of the silver nanoparticle is small. Finally the expression for $\mathbf{E}_{sph}$ is inserted. Note that the factors $\exp(i\omega t)$, is eliminated when taking the complex concjugate.

$$\sigma_{ext} = -\mathrm{Im}\{\frac{\mathrm{k}}{\epsilon_\mathrm{s}|\mathrm{E}_0|^2}\int_\mathrm{V} \mathrm{E}_0^*\mathrm{E}_0(\epsilon_\mathrm{m}-\epsilon_\mathrm{s})\frac{3\epsilon_\mathrm{s}(\epsilon_\mathrm{m}^* + 2\epsilon_\mathrm{s} - \mathrm{i}4\pi\mathrm{k}^3\mathrm{a}^3(\epsilon_\mathrm{m}^* - \epsilon_\mathrm{s})\frac{\mathrm{k}}{6\pi})}{|2\epsilon_\mathrm{s} + \epsilon_\mathrm{m}|^2}\mathrm{dV}\} \tag{4.26}$$

Since the integrand is not dependent on the sphere the expression under the integral can be moved outside the integral. Afterwards the expression is simplified.

$$\sigma_{ext} = -\mathrm{Im}\{\frac{3\mathrm{k}|\epsilon_\mathrm{m}|^2 - 3\mathrm{k}\epsilon_\mathrm{s}\epsilon_\mathrm{m}^* + 6\mathrm{k}\epsilon_\mathrm{s}\epsilon_\mathrm{m} - 6\mathrm{k}\epsilon_\mathrm{s}^2 - \mathrm{i}2\mathrm{k}^4\mathrm{a}^3(\epsilon_\mathrm{m}^* - \epsilon_\mathrm{s})(\epsilon_\mathrm{m} - \epsilon_\mathrm{s})}{|2\varepsilon_\mathrm{s} + \varepsilon_\mathrm{m}|^2}\int_\mathrm{V}\mathrm{dV}\} \tag{4.27}$$

The extinction cross section depends only on the imaginary part of the expression, therefore the real part can be neglected. Furthermore the integral is recognized as that of a simple sphere with radius, a.

$$\sigma_{ext} = -\{\frac{9k\varepsilon_s\mathrm{Im}(\epsilon_\mathrm{m}) - 2\mathrm{k}^4\mathrm{a}^3|\epsilon_\mathrm{m} - \epsilon_\mathrm{s}|^2}{|2\epsilon_s + \epsilon_m|^2}(\frac{4}{3}\pi a^3)\} \tag{4.28}$$

The final expression for the extinction cross section is given in Equation 4.29.

$$\sigma_{ext} = \frac{8}{3}\pi k^4 a^6|\frac{\epsilon_m - \epsilon_s}{2\epsilon_s + \epsilon_m}|^2 - 12\pi k a^3\frac{\epsilon_s\mathrm{Im}(\epsilon_\mathrm{m})}{|2\epsilon_s + \epsilon_m|^2} \tag{4.29}$$

4.4 Cross Section Graphs

Before considering the actual graphs an evaluation of Equation 4.29 is informative. The extinction cross section is the area shaded by the object in focus when exposed to a source of light. For macroscopic objects this extinction cross section equals the actual cross section as the approximation of geometrical optics and ray tracing is valid.

When the size of the object is in the nanoscale the geometrical description becomes faulty. The wave properties becomes dominant and properties as the ability of waves to bend corners ensues the need of another description of the extinction.

For particles in the nanoscale absorption and scattering overrules the physical cross section. The description of the sum of the absorption and

scattering of a particle is central to the optical properties. The extinction cross section is defined to be the virtual geometrical cross section the extinction from absorption and scattering would yield.

In Table 4.1 is the physical cross section and the extinction cross section from the model of silver nanospheres of various radii listed. As it can be seen the extinction cross section is greater than the physical cross section. This is however only true at the localized surface plasmon resonance (LSPR) peak. As an example the extinction cross section for the $10nm$ particle in this model a cross section is around $8 \cdot 10^{-18} nm$ at $600nm$.

Radius $[nm]$	Physical cross section $[m^2]$	Extinction cross section $[m^2]$
10	$3.14 \cdot 10^{-16}$	$1.64 \cdot 10^{-14}$
20	$1.26 \cdot 10^{-15}$	$7.5 \cdot 10^{-14}$
50	$7.85 \cdot 10^{-15}$	$2.2 \cdot 10^{-12}$

Table 4.1: A comparrasion between the physical cross section and the extinction cross section. The extinction cross section is taken from the LSPR peak. The resonance peak is measured at 405nm.

The location of the LSPR peak can be seen as the wavelength making the denominator of Equation 4.29 approach zero. This is given by $2\epsilon_s + \epsilon_m = 0$, it must be noted that the dielectric constant of silver is complex making this possible.

The wavelength is dependent solely on the refracive index of the solvent and silver. These values are connected with a certain degree of uncertainty, as values of different tables can vary a bit. Furthermore the refractive index of ethanol is dependent on the temperature. This results in a degree of uncertainty making it impossible to predict the precise location of the Plasmon Resonance peak.

For the silver nanoparticles in the various solutions of this report the spectrum from uv-vis spectroscopy is highly dependent on the extinction cross section of the silver nanoparticles. Therefore the information from comparison between the optical model of the silver nanoparticles and the experimental uv-vis spectrum is of great value when discussing sizes and shapes.

In order to conclude the model derived from the previous sections an expression of the dielectric constant is needed. In Section 2.4 it was stated that a material dependent model of the plasmon frequency was needed for the dielectric constant. In this report, however, an fitting curve will be made from a table of values for the refractive index. [Palik, 1985]

This was considered the optimal solution as model of the plasmon frequency would be rather comprehensive and not necessarily as precise as the one used here.

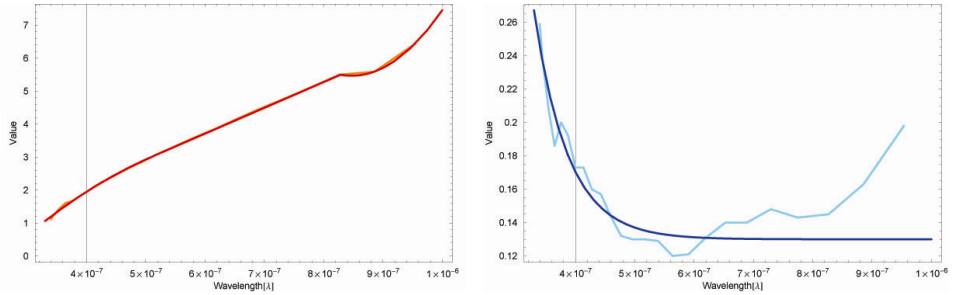

(a) (b)

Figure 4.1: The approximation of the real (4.1(a)) and imaginary part(4.1(b)) of the refractive index. In 4.1(a) the approximation becomes invalid at wavelengths above $800nn$*. This is however not important as the area, the plasmon resonance peak, in focus is around* $400nm$*.*

From plotting and piecewise fitting of the imaginary and real part of the refractive index of silver as a function of the wavelength, an approximation was made. The steps for this approximation is given in Appendix B.4 and the graph comparing the approximation and listed values are given in Figure 4.1.

The model for the small spherical silver nanoparticles derived in the previous sections is illustrated in the three graphs of Figure 4.2. The graphs are made for approximations of particles with radii of $10, 20$ and $50nm$.

From Figure 4.2(a) it is clear that for nanospheres of $10nm$ in radius the absorbance is completely dominant in the extinction cross section. When the radius becomes $20nm$ the scattering becomes increasingly dominant and for particles with radius $50nm$ the scattering is approximately as dominant as the absorption at radius $10nm$.

The model is only valid for very small spherical particles. In order to examine the range in which this model is precise a more complex description must be applied. Using several terms in Mie theory spherical nanoparticles with radius of $20nm$ would yield a small second peak at around $420nm$. [Pedersen, 2005]

For ellipsoidical nanoparticles a factor must be included that descibes the proportions in the different directions. This could also yield a double peak. [Sergey I. Bozhevolnyi, 2005]

This means that this model should only be applied for spherical nanoparticles smaller than $20nm$ in radius.

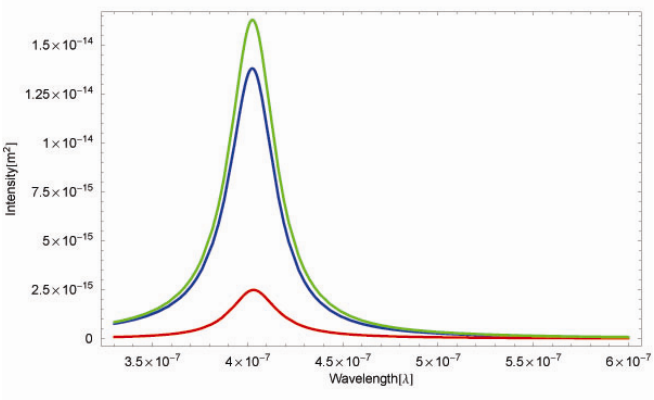

(a)

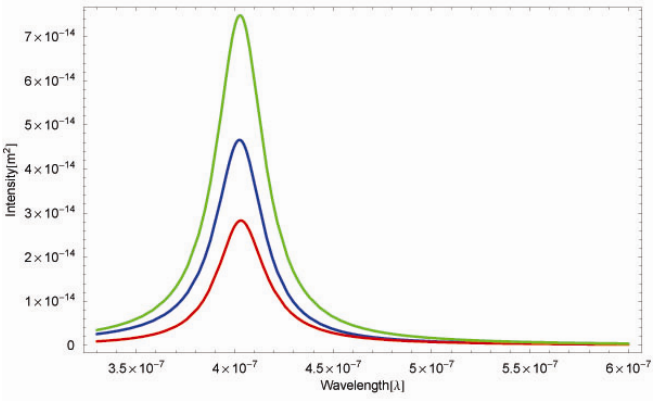

(b)

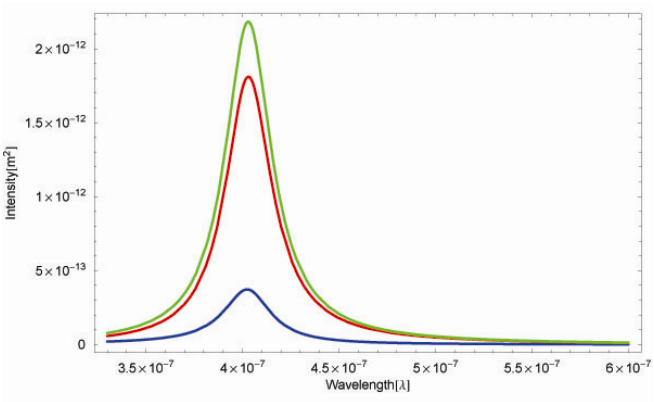

(c)

Figure 4.2: The calculated graphs for silver nanospheres of 10, 20, and 50nm in radius. The green curve is the extinction cross section, the blue is the absorption, and the red is the curve from the scattering.

Chapter 5

Data Processing

In this chapter the results obtained are presented. The chapter is split into sections describing the results obtained from each measuring method individually. The results from each method will also be discussed individually in each section.

5.1 Absorbance Spectroscopy

The results from absorbance spectroscopy of the samples listed in Table 3.2 are discussed in this section.

Figure 5.1 shows the five spectra, 1a, 1b, 1c, 1d and 1e. These samples are made at high concentration of silver nitrate. The peaks in all five spectra are relatively wide and they all show a double peak structure with the first and most intense peak located at $\sim 410nm$ and the second peak located at $\sim 450nm$.

It is clear that the sample which shows the highest peak intensity is 1c. Sample 1a was treated for 2 min and it shows the smallest peak intensity. The peak intensity increases as the samples are treated for longer time, but apparently this development stops at about 7 minutes (1c). At 10 minutes (1d) the peak intensity is drastically reduced and 20 minutes (1e) shows almost no change compared to 10 minutes.

Figure 5.2 shows the five spectra of 2a, 2b, 2c, 2d and 2e. These samples are made at low concentration of silver nitrate. By comparing these spectra with Figure 5.1 it is seen that the double peak structure has disappeared. This indicates that the double peak structure is related to the concentration of silver ions in the solution. It furthermore indicates that the silver nanoparticles are more homogenous compared to the spectra of 1a through 1e, because the spectra are generally more narrow. It is seen that the peaks are blue shifted to $\sim 400nm$. The intensity of

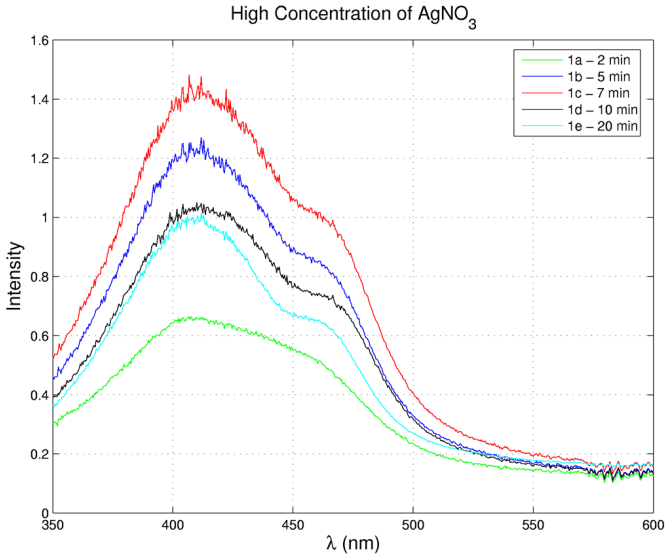

Figure 5.1: Absorbance spectra of the solutions with high concentration of silver. 1a has been exposed to microwaves at 160W in 2 min. and shows a peak at 407 nm, 1b in 5 min. and shows a peak at 412 nm, 1c in 7 min. shows the peak at 412 nm, 1d in 10 min. shows the peak at 411 nm and 1e in 20 min shows the peak at 412 nm. All spectra show a second peak at $\sim 450nm$.

In Figure 5.3 the spectra of 3a and 3b are shown. These spectra are both made from the same solution, but the spectra are recorded 15 min and 1 month respectively after heating in the microwave oven. The graphs show that both the peak and the intensity are not affected over time.

Figure 5.4 shows spectra of sample 4a and 4b. These samples have been treated with microwaves at 750 watt. A pattern similar to the pattern seen in Figure 5.1 and Figure 5.2 is observed. The sample at high concentration of silver (4a) shows a double peak structure with the first peak at $\sim 410nm$ and the second peak at $\sim 450nm$, while the sample at low concentration (4b) shows only one peak at $\sim 400nm$. The second peak in 4a is however not as distinct as in the samples which has been treated at a lower effect for longer time. Table 5.1 shows the difference in the peak placement.

The positions of the peaks from the spectra might indicate that the ratio of PVP vs. silver nitrate in the solution is important for the refractive index. It is likely to believe that synthesis with a low concentration of silver nitrate will give silver nanoparticles shielded with a more dense layer of PVP compared to silver nanoparticles synthesized with a low concentration of silver nitrate. This difference in the density of the PVP layer may explain why the position of the peaks is different in sample 1a-1e and 2a-2e.

The overall results from the absorbance spectroscopy clearly shows that

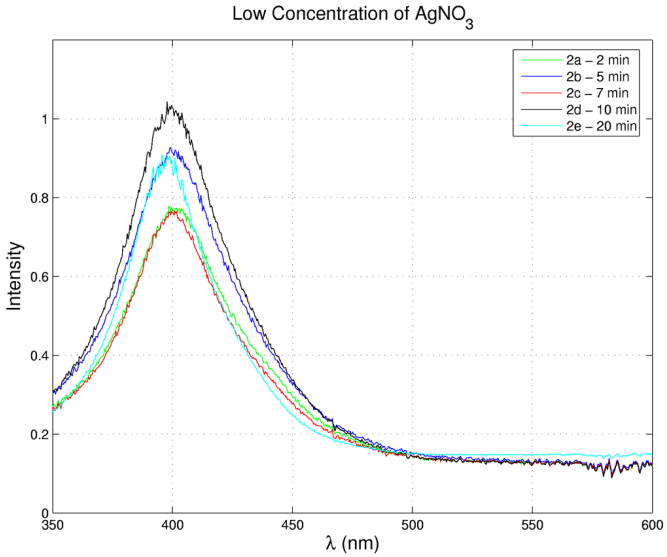

Figure 5.2: Absorbance spectra of the solutions with low concentration of silver. 2a has been exposed to microwaves at 160W in 2 min. and shows the peak at 401 nm, 2b in 5 min. shows the peak at 400 nm, 2c in 7 min. shows the peak at 400, 2d in 10 min. shows the peak at 399 nm and 2e in 20 min. shows the peak at 398 nm.

to obtain nanoparticles in small sizes and homogenous shapes it is preferable to use the low concentration of silver nitrate. High concentrations of silver nitrate causes a wide variety of shapes and sizes. From these results alone there can not be concluded anything about the sizes produced. Furthermore the spectra from samples 3a and 3b clearly shows that the synthesized silver nanoparticles are stable over time after treatment with microwaves.

When the spectra recorded from the synthesized silver nanoparticles are analyzed is it important to be aware of errors. One source of error could be the dilution of the sample. All the samples have been diluted 1:12 before testing to make it possible to record spectra with a reasonable noise level. It could be a possibility that the diluted samples do not give a scaled picture of the original sample.

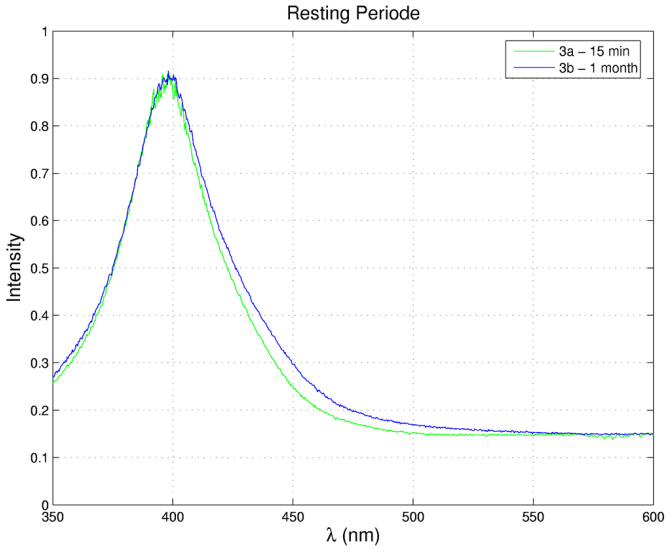

Figure 5.3: Absorbance spectra of the two solutions 3a and 3b. The spectra of 3a was taken shortly after the solution had been made and the peak is at 398 nm. The spectra of 3b was taken 1 month after and the peak is still at 398 nm.

Sample	Peaks [nm]	Sample	Peaks [nm]
1a	407/∼ 450	2a	401
1b	412/∼ 450	2b	400
1c	412/∼ 450	2c	400
1d	411/∼ 450	2d	399
1e	412/∼ 450	2e	398
3a	398	4a	407/∼ 450
3b	398	4b	404

Table 5.1: The peaks of the samples.

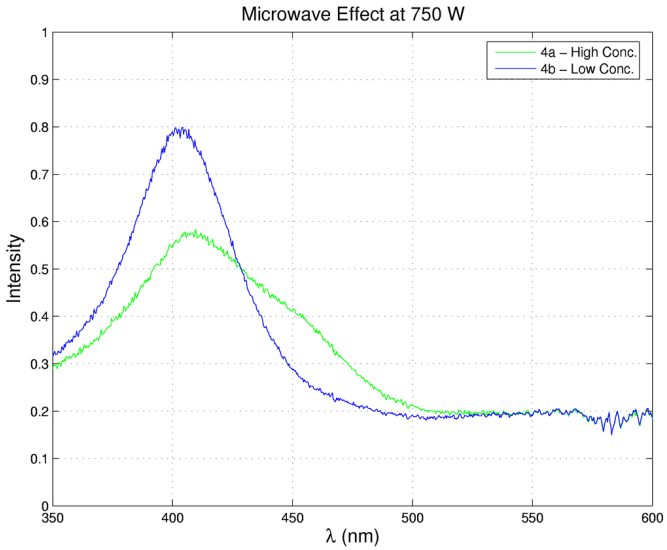

Figure 5.4: Absorbance spectra of the two solutions 4a and 4b. 4a is at high concentration of silver and shows a peak at 407 nm. 4b is at low concentration and shows a peak at 404 nm. Each of the two samples are treated with microwaves at 750 watt.

5.2 Dynamic Light Scattering

This section describes and discusses the results obtained from DLS. The results are shown as an error bar diagram in Figure 5.5. The diagram shows the average diameter measured in the respective sample and a vertical bar showing the deviation from the average diameter.

From the diagram it can be seen that the average diameters are between 20 and $30nm$. The distribution extends from $\sim 6nm$ to as much as $\sim 70nm$. However, only very few particles with diameters above $\sim 50nm$ and below ~ 10 was detected. This observation conflicts the aim of synthesizing particles at $10nm$, but can be explained by the fact that DLS is incapable of distinguishing between PVP and silver. Because the silver nanoparticles are capped with PVP stretching out from the particle as tentacles, the diameter is increased by an amount approximately equal to two times the thickness of the PVP polymer chain layer. The thickness of the PVP polymer chain is not known, but it can be said to be significant compared to nanoparticles of $10-15nm$ in size as the molecular weight of the PVP used is $40,000g/mole$.

There is no clear pattern in the results obtained. Sample 1a through 1e varies by the microwave treatment period from 2 to 20 minutes, but the size of the particles measured by DLS does not vary accordingly. Sample 2a through 2e shows a slight pattern as the average diameter seems to be decreasing from $\sim 43nm$ to $\sim 25nm$. This is however a strong contradiction to the theory that the particles grow when treated with microwaves. A possible explanation could be that PVP forms aggregates and these aggregates are destroyed when the solution is heated. This would account for the decrease in size from large particles to smaller ones.

No clear difference between the samples at high (1a-1e) and low (2a-2e) silver nitrate concentration is observed. It is sensible to assume that when the amount of PVP is kept constant and the amount of silver nitrate is increased, larger particles would result due to agglomeration and uncontrolled growth. According to these results however, this does not seem to be the case.

Sample 4a and 4b was treated for $30sec$ at $750watt$ and according to the DLS results this yields large particles with an average diameter in the range $50-60nm$. When the solution is mixed the PVP aggregates and form large particles. Upon heating of the solution, the large PVP aggregates are destroyed and form micelles around silver. $750watt$ for $30secs$ might not provide enough energy to destroy all the PVP aggregates, and this could explain why particles between 50 and 60 nm are observed in the solution.

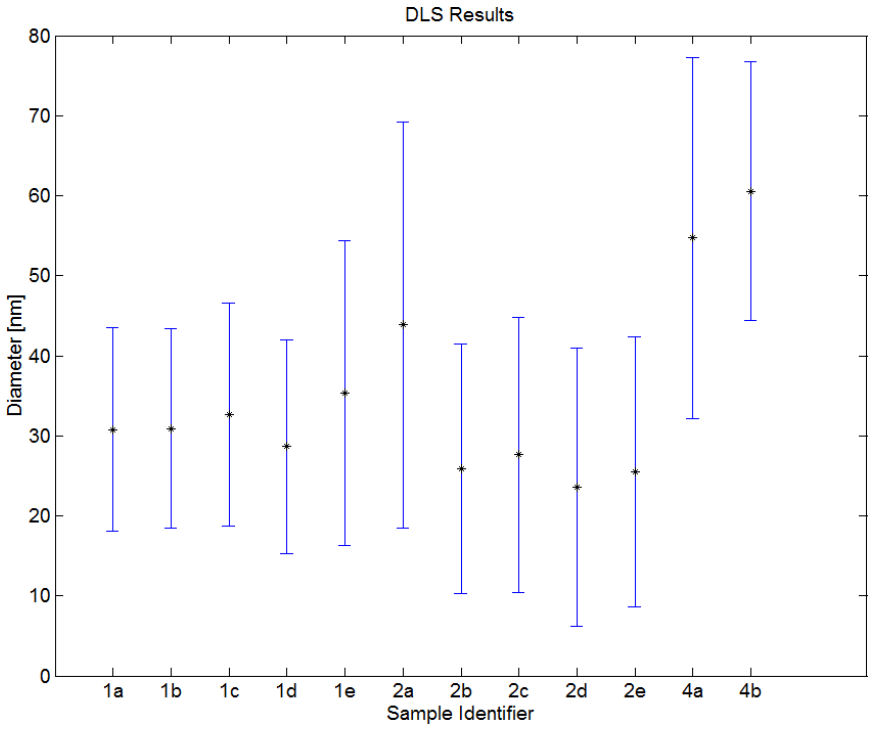

*Figure 5.5: All the results obtained from DLS. The average diameter measured and the deviation from the average diameter of the sample are shown. The average diameter is marked with a *.*

5.3 Scanning Electron Microscopy

The pictures from the SEM experiment showed silver nanoparticles distributed on the wafer as expected. The wafers was coated with the silver nanoparticle solution from sample 2d and 2e. In addition, one wafer was coated with silver solution which had not been treated with microwaves.

The first wafer shown in Figure 5.6(a) was coated with silver nanoparticles that had not been treated with microwaves. This sample did not show any traces of silver nanoparticles. Instead, crystal-like structures at a size of about $1\mu m$ covered the picture.

The wafer treated with sample 2d showed spherical nanoparticles, quite close distributed, with approximately similar diameters. This result is shown in Figure 5.6(b). The exact size of the nanoparticles is difficult to measure because of the rough resolution of the pictures. However, an approximated value was determined in order to correlate the pictures from each other. The particles on this wafer was measured to be around 18 ± 5 nm in diameter.

In sample 2e the size of the particles seems larger than in sample 2d, see Figure 5.6(c). Using the same method for determining the size of the

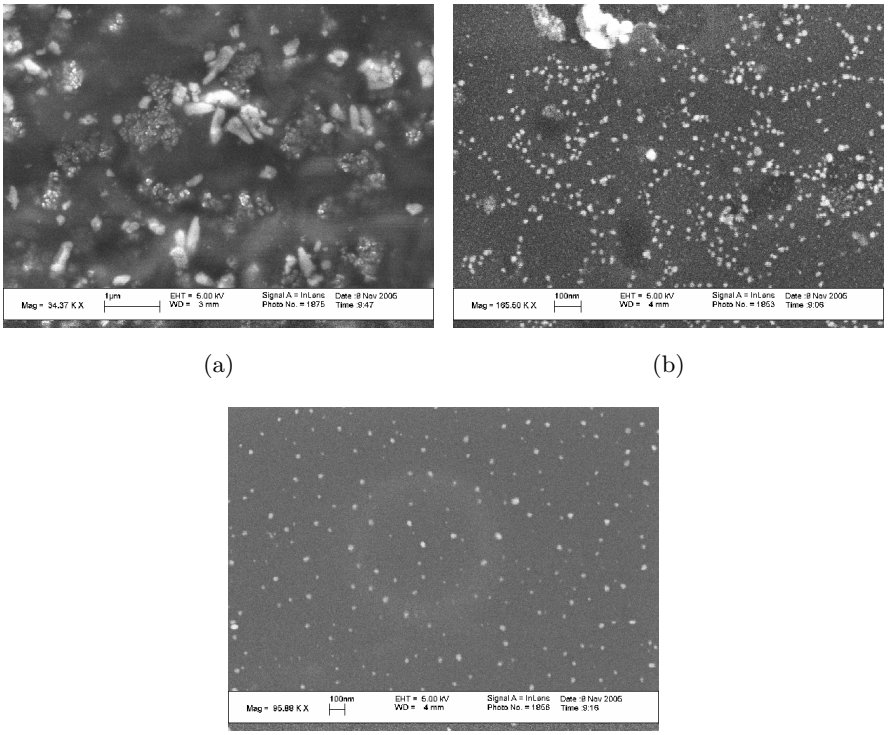

(a) (b)

(c)

Figure 5.6: 3 SEM pictures of silver nanoparticles. (a) a wafer coated with silver nitrate/PVP solution which had not been treated with microwaves. (b) solution treated 10 minutes in microwave oven (sample 2d). (c) solution treated 20 minutes (sample 2e).

particles resulted in an approximated value of 30 ± 10 nm, indicating that the particles have grown.

5.4 Atomic Force Microscopy

Sample 2e was analyzed using AFM. The AFM pictures of the sample were analyzed and slightly modified. A raw picture of the topography is shown in Figure 5.7.

Single silver nanoparticles are shown in Figure 5.8. The 3D zoom was performed using the software.

The width of the silver nanoparticles was measured using the software. The width was determined at three different locations on the particle. The pictures in Figure 5.9(a) show cross-sectional views of the particle three different places. The axes are equivalent.

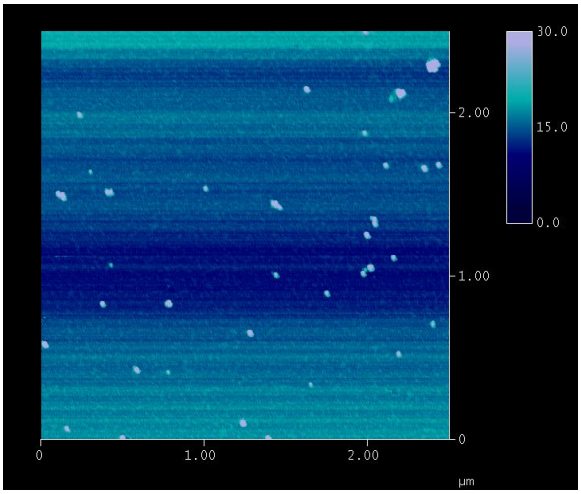

Figure 5.7: A raw AFM picture of the wafer coated with silver nanoparticles

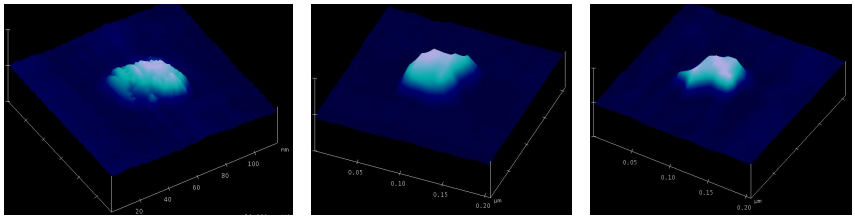

(a) (b) (c)

Figure 5.8: AFM pictures of three different single silver nanoparticles.

The height of the silver nanoparticles was also measured using the software. The height was determined three different places on the particle. The pictures in Figure 5.9(b) show cross-sectional views of the particle three different places. The axes are equivalent.

15 arbitrarily chosen particles were analyzed this way in order to measure the average width and height of the particles.

Also, sample 1e was tested using AFM, and the results are shown in Figure 5.10. Unfortunately, it seems that the silver nanoparticles had clustered together, or that the wafers were not completely cleaned for PVP, therefore the results are hardly useful. The raised platforms on the pictures are $\sim 100nm \pm 50$ in diameter and $\sim 20nm$ in height.

When using AFM it is important to remember that the shape of the tip may cause misleading cross sectional views of the sample as demonstrated in Figure 5.11. Therefore pictures taken with AFM have to be analyzed and machined in relation to the specific AFM apparatus.

For the AFM apparatus used for these results, $10nm$ has to be subtracted from the diameter measurements to correct for the errors caused by the

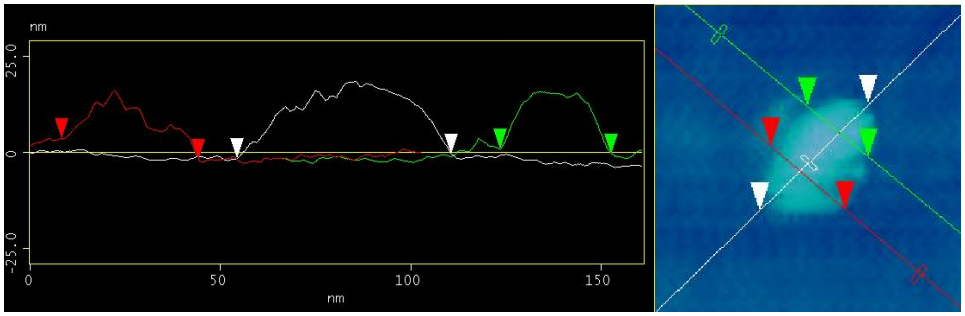

(a)

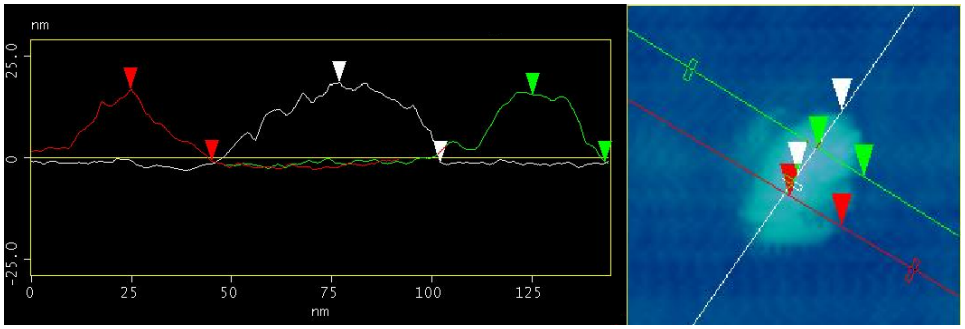

(b)

Figure 5.9: (a) The width of a particle is measured. A cross sectional view of the particle is obtained using the software and the triangles are manually placed at the particle edge, and the software displays the length between the triangles. (b)The height of a particle is measured using the same method

shape of the tip. Also, one has to allow for an eventual layer of PVP on the wafer and on the nanoparticles which could distort the results. This is however difficult to include in the data processing.

Analysis of the AFM results yielded particles of average size of 37 nm in width and 18 nm in height. These results are corrected for the width of the AFM tip.

5.5 The Bactericidal Effect

In this section the results of the bacteria experiments will be presented and discussed. Before starting the main experiments it had to be determined if the stabilizer used had an effect on the bacteria. The results showed that the PVP had no effect on the bacteria growth.

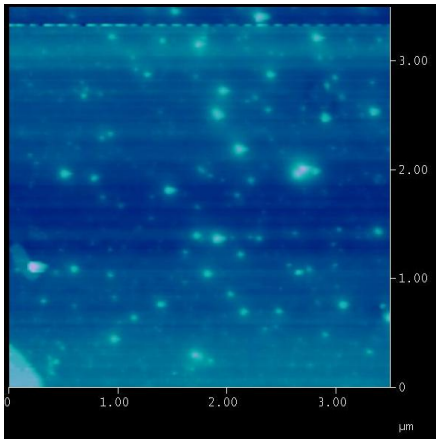

(a)

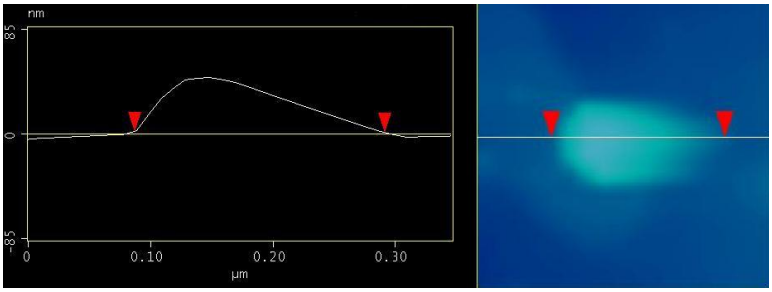

(b)

Figure 5.10: AFM pictures of sample 2e.

5.5.1 The Best Suited Treatment Method

The first experiment was carried out to determine in which way the immobilization of the silver nanoparticles had to be done to yield the best results. Three methods was tested; Placement of nanoparticle coated glass plate and filter paper on the LB plates, and direct deposition of silver nanoparticles. The three pictures in Figure 5.12 show the results of these experiments.

The glass plate result shown in Figure 5.12(a), shows at first glance that the silver nanoparticles have a bactericidal effect because no bacteria are observed beneath the glass plate. But when taking the reference experiment into perspective it shows that the bacteria cannot live in the area under the glass plate due to asphyxiation. The area just around the glass plate is also bacteria free and this is probably a result of some of the silver nanoparticles from the glass plate being dissolved in water from the medium.

The filter paper result shown in Figure 5.12(b), shows a piece of filter paper treated with nanoparticles and placed on top of the bacteria. This allows the bacteria to breath as the filter paper is non air proof. The result

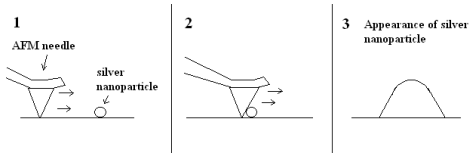

Figure 5.11: A schematic demonstration of the disadvantage of AFM

showed that the bacteria were killed in the area around the paper, like the method of the coated glass plate, making it difficult to interpret the results. In order to collect useable data the filter paper will have to be removed, causing some of the bacteria to be removed. This makes it difficult to see if bacteria has survived.

The results of direct deposition is shown in Figure 5.12(c) and shows that the silver nanoparticles cause the death of all the bacteria on the nanoparticle coated side. It is certain that the bacteria death is not due to non vaporized ethanol. This can be seen by comparison with the reference experiment which showed that all the bacteria survived proving that the ethanol has been successfully removed.

The overall result of the experiment was that the method of direct treatment was the best both in terms of giving the bacteria the best growth conditions and in making the data collecting easy and straight forward, minimizing the probability for errors. Therefore it was chosen to be the method used in later experiments.

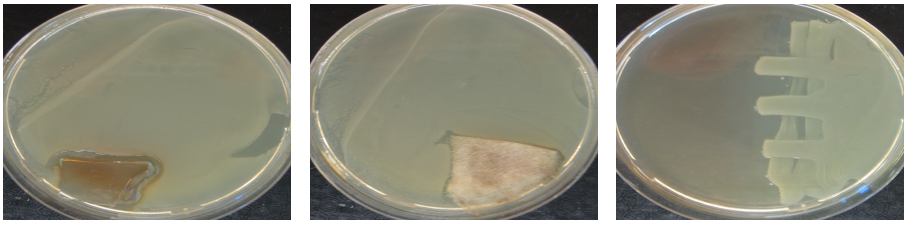

(a) (b) (c)

Figure 5.12: The tested methods for the immobilization of silver nanoparticles. (a) LB plate with a glass plate to immobilize the nanoparticles. (b) LB plate with a piece of filter paper treated with nanoparticles. (c) LB plate with direct treatment of silver nanoparticles.

5.5.2 The Optimal Dilution

The purpose of this row of experiments is to determine how much a sample of low silver to PVP ratio can be diluted and still yield bactericidal properties. The dilution wanted is one where some bacteria survive.

Figure 5.13(a) shows the result from a dilution of 1:4; all bacteria in the area treated with nanoparticles has died. The Figure 5.13(b) shows the result from a dilution of 1:8; some colonies of bacteria has survived in the treated area. The Figure 5.13(c) shows the result from a dilution of 1:12; all bacteria in the treated area has survived. These results shows that the dilution that should be used to determine the optimal production method is 1:8.

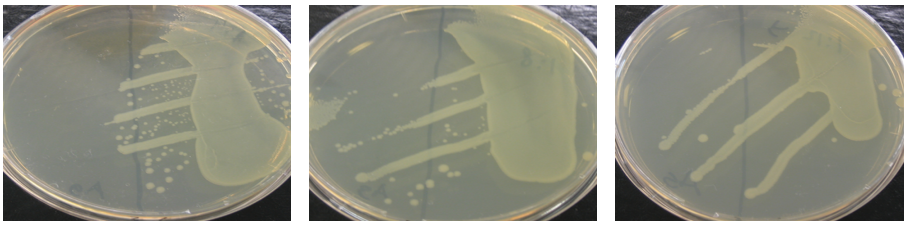

(a) (b) (c)

Figure 5.13: LB plate with a ratio between solute and the silver nanoparticle sample of (a) 1:4, (b) 1:8, (c) 1:12.

5.5.3 The Production Method Best Suited for Inhibiting Bacterial Growth

These experiment was carried out to determine the optimal ratio between PVP and silver in the base solution. Furthermore it was intended to test which effect the time in the microwave oven has on the bactericidal effect. All of these experiments turned out to be difficult. Even though the same amount of solution was used in the experiments it was not possible to replicate the results from the first experiment. This could be explained by the difficulties in covering the exact same area with silver nanoparticles on all plates making the $[Ag/cm^2]$ vary from experiment to experiment. Another possibility could be the moist of the medium used. If the amount of water present on the surface of the medium is high then the relative concentration of silver nanoparticles is low allowing more bacteria to survive. If on the other hand there is only little water present, the relative concentration would be high and the bacteria would die. It is also possible that the silver nanoparticles are able to migrate into the medium. If this is the case then the time, in which the plates are left without bacteria, could make the result differ.

As a result of the fact that the experiment could not be repeated the search for the best production method did not give useful results. The attempts on collecting useable data included experiments where a 1:8 dilution was at first observed to kill all the bacteria. Then another row of

experiments was set up using the same dilution, now showing no sign of a bactericidal effect. Another experiment yielded results showing that also a 1:10 dilution caused the death of all bacteria.

Chapter 6

Discussion

In this chapter the individual results obtained are discussed in relation to each other. Possible explanations on the accordance and contradictions between results are given.

6.1 Evaluation of Measuring Methods

Nanotechnological measuring methods are by their nature difficult to evaluate with respect to their validity. Therefore it is crucial to analyze and discuss the results both independently and in relation to each other. Especially the size and shape of the silver nanoparticles are important matters in this report, therefore the possible measuring problems are important to be aware of.

When the silver nanoparticles are suspended in the solution the PVP molecule stretches away from the nanoparticle. This explains the rather large size distribution measured by DLS. Because DLS measurements are performed on the nanoparticle solution, the diameter of the particle will be measured as two times the thickness of the PVP layer plus the diameter of the actual particle.

When the particle is placed on a wafer and the ethanol is removed the PVP layer on the particle will collapse on the surface. This means that the diameter will decrease compared to that measured by DLS, but it is still larger than that of the actual particle. The results obtained by AFM is the particle size with the layer of PVP on the surface. This result is still closer to the actual size of the particle than that measured by DLS. Furthermore the size is measured as the difference in height between the wafer surface and the top of the particle. This is done to prevent taking the size of the tip and the PVP layer into consideration. However, this also includes a problem if the solution contains a high amount of PVP; it would settle on the surface of the wafer and the particle making the results doubtful.

In order to obtain data telling something about the actual particle beneath the PVP layer the results from SEM can be used. Nanoparticles appear much brighter in the SEM images than PVP, because silver has a higher atomic number than the atoms constituting PVP. Therefore only the silver nanoparticles are seen in the SEM images.

Hence, the particle size measured using the SEM apparatus will be used to support the data obtained from the AFM, DLS, and absorbance experiments.

6.2 Size And Shapes

This section discusses the obtained data in relation to size and shape of the synthesized silver nanoparticles. The size is discussed is relation to the absorbance spectroscopy, AFM, SEM, and DLS experiments, and the accordance of these results to the optical model is discussed. Lastly, the dependence of size on microwave treatment period is discussed.

6.2.1 The Optical Model in contrast to The Absorbance Spectra

The absorbance spectroscopy is a fast way to obtain data of silver nanoparticle solution. However, these data alone does not tell much about the silver nanoparticles. A correlation with an optical model must be made.

The absorbance graph of the solution made from the low concentration of $AgNO_3$ can be seen in Figure 5.2, it shows a single clear LSPR peak. According to the optical model this occurs for spherical particles below $40nm$ in diameter. The peak is placed at $400nm$, a little shorter than in the optical model. However this exact placement is subject to the uncertainty of the refractive index of silver and ethanol. Furthermore the silver nanoparticles are covered with a PVP layer that might yield a shift in the refractive index. The degree of this error has, however, not been investigated.

A comparison of the width of the peak of Figure 5.2 with the optical model shows a wider peak than anticipated. This could be because there is a distribution of radii in the solution while the optical model is calculated for one particle of radius 10, 20, or 50 nm.

In Figure 5.1 the absorbance graph of the high concentration of $AgNO_3$ is displayed. There is a peak at around $410nm$ and a second peak around $450nm$. The optical model developed in Chapter 4 does not predict this absorbance spectrum. A more complex optical model is needed for a good description of the double peak and therefore the evaluation of this graph will be subject to a larger degree of uncertainty.

For larger particles, a more complex Mie scattering theory must be applied. For silver nanoparticles with radii in the range of $50nm$ a broad peak

at around $460nm$ would occur [Pedersen, 2005]. A third peak at a shorter wavelength would also occur. Without thorough treatment of the Mie scattering theory it is however not possible to conclude anything final in regards to Figure 5.1.

Another possibility is a change in shape of the particles, e.g. ellipsoidal particles. Ellipsoidal particles would yield multiple LSPR peaks dependent on the orientation of the particles. This has however not been investigated in the optical model.

A third possibility is the agglomeration of multiple silver nanoparticles yielding more randomly sized and shaped particles. In Section 2.3.2 the repulsive forces was described of two nanoparticles stabilized with polymer layers approaching each other. This description stated that when the particles was not fully covered they would experience a weaker repulsive force when interpenetrating making it easier to agglomerate.

This consideration supports the idea of agglomerated nanoparticles in the solution of high concentration. Agglomerated nanoparticles could also yield a double peak but the developed optical model does neither cover this.

Figure 5.3 shows that the shape of the absorbance graph changed little after one month. This indicates that the spherical nanoparticles remained stable in suspension when first synthesized.

In Figure 5.4 it was tested if higher effect for shorter time could be used for synthesizing nanoparticles of $10nm$ in size. The spectra show the same peaks and shapes as in Figure 5.1 and Figure 5.2, and this indicates that spherical nanoparticles have been produced.

6.2.2 The Particle Size

In order to check if a comparison between the absorbance spectra and the optical model gives a reliable picture of the size distribution it is necessary to take the results from the DLS, SEM and AFM analyses into consideration. Since the DLS results are affected by the PVP layer shielding the silver nanoparticles they will not be discussed any further.

By a comparison of the optical model and the absorbance spectra from sample 2 it has been estimated that the synthesized silver nanoparticles was below 30nm in diameter. Analysis of the AFM pictures yield particles with an average size of $18nm \pm 5nm$, which indicate that the results from the comparison of the optical model and the absorbance spectra are correct. The SEM picture of sample 2d also showed spherical particles with an average size of 18nm, which furthermore indicates that a comparison of the absorbance spectra and the optical model can be used to estimate the sizes of the silver nanoparticles. The SEM picture of sample 2e showed spherical particles with an average size of $30nm \pm 10nm$. This correspond to the predictions made from the optical model.

From the AFM picture of sample 1e it can be seen that the silver nanoparticles no longer are spherical, which means that the optical model cannot be used to estimate the size of the particles. The AFM picture can however be used to explain the double peak in Figure 5.1. The double peak could be a consequence of the nanoparticles which are not spherical.

6.2.3 Microwave Treatment Period vs Size

From the results of absorbance spectroscopy, DLS, and AFM it is difficult to describe any relation between exposure time in the microwave oven versus the sizes of the synthesized silver nanoparticles.

The absorbance spectra recorded from each sample does not change in shape but only in intensity when exposure time is varied. This indicates that the size of the silver nanoparticles does not exceed 30 nm in diameter. The results from DLS are adversely affected by the PVP layer which makes it impossible to describe any relation between exposure time and size of the silver nanoparticles. Only one AFM picture of sample 1 and one picture of sample 2 was made, which makes it very difficult to describe the relation between exposure time and size from the AFM results. More AFM images of the same sample at different treatment times would have made this comparison possible.

The results of SEM analysis give a picture of the silver nanoparticle growth when the solution is exposed to microwaves. It is clear that the silver nanoparticles grow bigger when the solution is exposed to microwaves for a longer time. Unfortunately, the SEM pictures also show that the distribution gets wider when the solution is exposed to microwaves for a longer time, which makes this synthesis method improper for production of large silver nanoparticles

6.3 Bactericidal Effect In Relation To Silver Nanoparticle Size

Because the best production method for producing bactericidal silver nanoparticles could not be determined, the relation between size and the bactericidal properties could not be directly established.

The examination of samples with SEM showed that the nanoparticle solution contained a wide size distribution with particles around $20nm$. As explained in Section 2.6.4 the article [Morones et al., 2005] describes that particles beneath the size of $10nm$ yield the best bactericidal properties. This differ from the results obtained in this project as the known size distribution of the produced nanoparticles indicate that most of the synthesized nanoparticles are too large to yield this effect. One explantation can be that

the solutions contain some silver nanoparticles beneath $10nm$. Another option is that the bactericidal effect could be due to silver ions released from the nanoparticles.

In this project it could not be determined if the bactericidal effect was due to the effect of silver nanoparticles or due to the effect of silver ions.

Chapter 7

Conclusion

In this project the production, optical properties, and bactericidal effect of silver nanoparticles have been examined. This chapter concludes on the problem statement in Section 2.9.

In order to determine the size dependence of the silver nanoparticles in relation to the bactericidal effect a series of experiments was carried out. Due to problems concerning attempts to repeat the experiments it was not possible to establish a size relation to the bactericidal effect.

It has been shown that the size distribution of small spherical silver nanoparticles can be estimated by comparing the absorbance data with the optical model. This estimation is supported by comparison with the AFM and SEM results. DLS was used to measure the size of the particles, but due to the PVP layer shielding the nanoparticles this method is not appropriate.

In this project the ratio between silver nitrate and PVP showed to cause the most radical change in size, and the exposure time showed only little effect on the size. By varying the silver nitrate/PVP ratio the process of synthesizing nanoparticles can be optimized.

Bibliography

[Alcamo, 1997] Alcamo, I. E. (1997). *Fundamentals of Microbiology 5. edition*. Benjamin Cummings.

[Braydich-Stolle et al., 2005] Braydich-Stolle, L., Hussain, S., Schlager, J. J., and Hofmann, M.-C. (2005). In vitro cytotoxicity of nanoparticles in mammalian germline stem cells. *Toxicological Sciences*.

[Britannica.com, 2005a] Britannica.com (2005a). Cell. `http://search.eb.com/eb/article-9106125?query=cell&ct=`.

[Britannica.com, 2005b] Britannica.com (2005b). Nanotechnology. `http://search.eb.com.zorac.aub.aau.dk/eb/article-9384821?query=nanotechnology&ct=`.

[Cao, 2004] Cao, G. (2004). *Nanostructures and Nanomaterials*. Imperials College Press.

[Chou et al., 2005] Chou, K.-S., Lu, Y.-C., and Lee, H.-H. (2005). Effect of alkaline ion on the mechanism and kinetics of chemical reduction of silver. *Science Direct*.

[Frattini et al., 2005] Frattini, A., Pellegri, N., Nicastro, D., and de Sanctis, O. (2005). Preparation of polychrome silver nanoparticles in different solvents. *Journal of Materials Chemisthy*.

[Grijalva et al., 2005] Grijalva, A. S., Urbina, R. H., Silva, J. F. R., and Borja, M. A. (2005). Ethylene glycol silver nitrate polyvinylpyrrolidone. *Science Direct*.

[Jain and Pradeep, 2004] Jain, P. and Pradeep, T. (2004). Potential of silver nanoparticle-coated polyurethane foam as an antibacterial water filter. *Wiley InterScience*.

[Jiang et al., 2004] Jiang, Z.-J., Liu, C.-Y., and Sun, L.-W. (2004). Catalytic properties of silver nanoparticles supported on silica spheres. *American Chemical Society*.

[Klein and Furtak, 1986] Klein, M. V. and Furtak, T. E. (1986). *Optics*. Wiley.

[Lodish et al., 2000] Lodish, H., Berk, A., Zipursky, S. L., Matsudaira, P., Baltimore, D., and Darnell, J. (2000). *Molecular Cell Biology*. W.H Freeman And Company.

[McFarland and Duyne, 2003] McFarland, A. D. and Duyne, R. P. V. (2003). Single silver nanoparticles as real-time optical sensors with zeptomole sensitivity. *Nanoletters*.

[Microtrac.com, 2005] Microtrac.com (2005). Microtrac dynamic light scattering. `http://www.microtrac.com/dynamicscattering.cfm`.

[Morones et al., 2005] Morones, J. R., Elechiguerra, J. L., Camacho, A., Holt, K., Kouri, J. B., Ramírez, J. T., and Yacaman, M. J. (2005). The bactericidal effect of silver nanoparticles. *Nanotechnology*.

[ouh.dk, 2005] ouh.dk (2005). Sårbehandling med produkter. `http://www.ouh.dk/wm137648#bm%2070209`.

[Palik, 1985] Palik, E. D. (1985). *Handbook of Optical Constants of Solids*. Academic Press, New York.

[Pedersen, 2005] Pedersen, T. G. (2005). Mie scattering theory. *Notes for nano3 2005 AAU*.

[proteinchemist.com, 2005] proteinchemist.com (2005). Protein chemist - dynamic light scattering. `http://www.proteinchemist.com/dls/dls.html`.

[samsung.com, 2005] samsung.com (2005). Samsung silver nano health system gives free play to its "silver" magic. `http://www.samsung.com/he/presscenter/pressrelease/pressrelease_20050329_0000109066.asp`.

[Sergey I. Bozhevolnyi, 2005] Sergey I. Bozhevolnyi, A. B. E. (2005). Surface plasmon polaraton scattering by small ellipsoid particles. *Science Direct*.

[Wang et al., 2005] Wang, H., Qiao, X., Chen, J., Wang, X., and Ding, S. (2005). Mechanisms of pvp in the preparation of silver nanoparticles. *Science Direct*.

Appendix A

Dynamic Light Scattering

Dynamic Light Scattering (DLS) is a measuring technique which is used for determination of particle size and particle size distribution.

In overall terms, the DLS instrument is build up as schematized in Figure A.1. The laser beam is send through a stainless steel tube towards the particle suspension through the wave guide tip. Here is a part of the beam reflected directly backwards to the photo detector, whereas another part of the light is send towards the solution. Some of the light is backscattered and send back to the photo detector through the stainless steel tube. The photo detector uses the arriving light to determine the size of the particles in the solution.

The technique makes use of the shift of the frequency of light when it interacts with particles, and the fact that this change depends on the particle size. In order to understand the motion of the particles in a solution we introduce the so-called *Brownian Motion*, which is a result of the *Kinetic Molecular Theory*; the molecules of a solution that are much smaller than the dissolved particles can impart a change to the direction of the particle and its velocity.

Thus, when small particles are suspended in a resting fluid solution, they tend to move in a random pattern around each other. Observations made by optical microscopy on relatively large particles shows that larger particles tends to move slower than smaller particles. This is a direct result of the conservation of impulse theory.

When a laser at a known frequency is pointed at the solution, the light impinges the particles and induces an oscillating polarization of their electrons. The particles then serve as a secondary source of light and subsequently radiate light. This causes a frequency- and intensity shift of the light leaving the solution, which is dependent on the composition of the solution.

Due to their higher average velocity, smaller particles cause a greater shift in the light frequency than larger particles. The frequency-shifted light

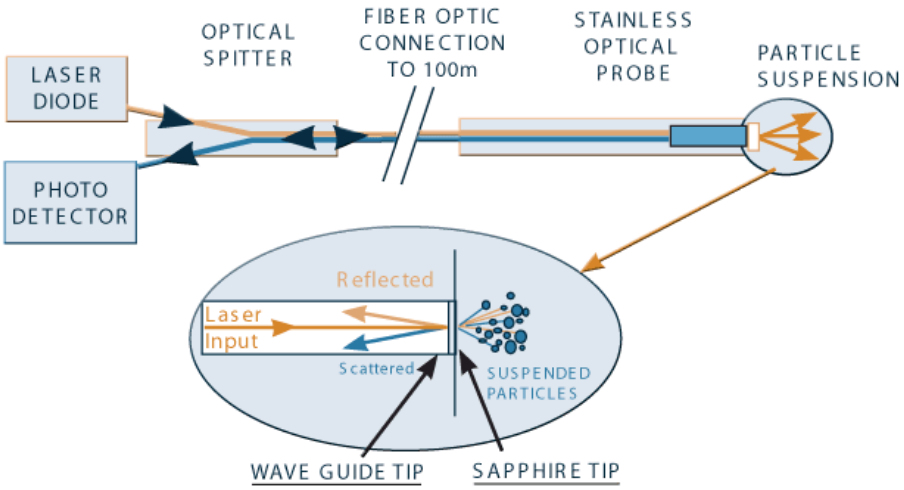

Figure A.1: A schematic view on a DLS apparatus. A laser diode emits light through the tube towards the solution. Part of the beam is reflected back towards the detector, while the other part is send into the solution where it is reflected and pointed back to the detector. From [Microtrac.com, 2005]

is mixed with stable, unshifted light and send towards a detector. The unshifted light originates from the laser, a part of which is reflected in the instrument to the detector. This light acts as a stable reference point or baseline for the scattered, shifted light from the solution. The interference of the reflected and shifted light is determined in the detector and is used to determine the sizes of the particles present. [Microtrac.com, 2005]

Studying Figure A.2 one can briefly understand how the detector measures the particle size.

The light intensity is $I(t)$ at time t (A). At the time $t+\tau$ (B), which is a very small time later than t, the diffusing particles will have new positions and the intensity at the detector will have a value $I(t+\tau)$. The detector saves the values for $I(t+\tau)$ numerous times (C), and eventually the software calculates the autocorrelative function from the discrete values.

The autocorrelative function describes how a given measurement relates to itself in a time dependent manner:

$$r_\tau = \frac{\sum_{i=1}^{N-k}(Y_i - \overline{Y})(Y_{i+k} - \overline{Y})}{\sum_{i=1}^{N}(Y_i - \overline{Y})^2} \tag{A.1}$$

At time zero, $r = 1$ i.e. there is 100% correlation. As time progresses, the autocorrelation diminishes reaching zero as there is no more similarity between starting and ending states.

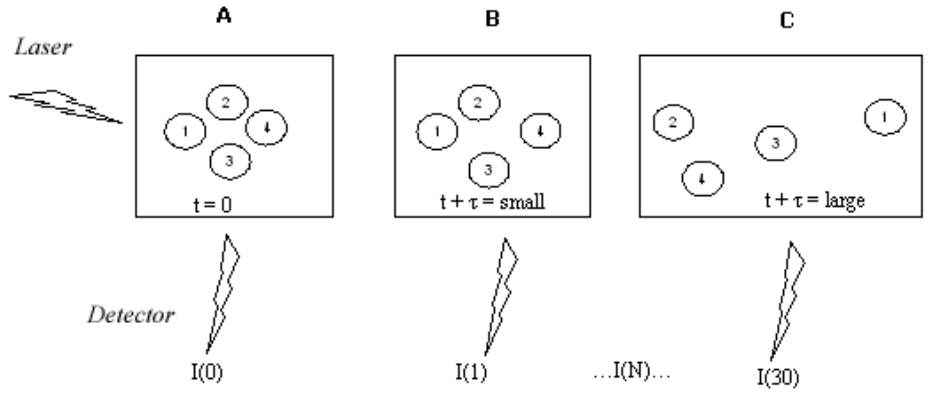

Figure A.2: A schematic DLS experiment. The particles in a solution (1,2,3 and 4) moves in a random pattern as a function of time t, and the intensity I of the emitted light is measured by the detector. From [proteinchemist.com, 2005]

The decay of the autocorrelation is described by an exponential decay function Equation A.2 which relates the autocorrelation to the diffusion coefficient D and the measurement vector K:

$$G(\tau) \propto e^{-2DK^2\tau} \tag{A.2}$$

where K is given by

$$K = \frac{4\pi n}{\lambda} \sin \frac{\theta}{2} \tag{A.3}$$

all the coefficients are constants for the equipment and solution: n is the refractive index of the solution. λ is the wavelength of the laser. θ is the angle of scattering measurement.

By fitting the points of autocorrelation to the function $G(t)$, the diffusion coefficient can be measured and related to the equivalent sphere of diameter d using the Stokes - Einstein equation:

$$D = \frac{k_B T}{3\pi\eta d} \tag{A.4}$$

where k_B is the Boltzmann constant, T is the temperature of the solution, η is the diluent viscosity and d is the diameter of the particles. Hence, d is the only variable and can be determined. [proteinchemist.com, 2005]

Appendix B

Calculations from the Optical model

In the chapter of the optical model a number of derivations was skipped. Those will be thoroughly explained in this appendix.

B.1 The derivation of G

The derivation of the identity from Equation 4.17 starting from the definition of G, Equation B.1.

$$G = [\frac{1}{k^2}(\nabla\nabla + k^2 I)]g(r) \tag{B.1}$$

When expanding the parenthesis 2 terms are achieved, and $\nabla\nabla g(r)$ shall be treated firstly. Instead of $g(r)$, g will be written keeping in mind that it is a function of r. When taking the gradient of g, the derivative with respect to x will be treated firstly and the expanded to the 3 dimensional problem.

At first some simple expressions must be derived.

$$\begin{aligned} \frac{\partial g}{\partial x} &= \frac{\partial g}{\partial r}\frac{\partial r}{\partial x} \\ &= \frac{x}{r}g(r)(-\frac{1}{r} - ik) \end{aligned} \tag{B.2}$$

From connecting the three terms of Equation B.2 in $\nabla g(r)$ Equation B.3 is achieved.

$$\nabla g = (-\frac{1}{r} - ik)g(\frac{x}{r}\hat{x} + \frac{y}{r}\hat{y} + \frac{z}{r}\hat{z}) = \hat{r}(-\frac{1}{r} - ik)g \tag{B.3}$$

Now the second gradient is evaluated using the same procedure and the expressions of Equation B.2.

$$\begin{aligned}\frac{\partial}{\partial x}(\nabla g) &= \frac{\partial}{\partial x}(-\frac{1}{r}-ik)g) + \hat{r}\frac{\partial}{\partial x}((-\frac{1}{r}-ik)g) \\ &= (\frac{1}{r}\hat{x}-\frac{x}{r^2}\hat{r})(-\frac{1}{r}-ik)g + \hat{r}g(\frac{x}{r^3}+(-\frac{1}{r}-ik)^2 \end{aligned} \quad \text{(B.4)}$$

From Equation B.4 the components of y and z is once again evaluated and connected.

$$\hat{x}\frac{\partial}{\partial x}(\nabla g) = g(\frac{\hat{x}x\hat{r}}{r}(-k^2+\frac{3ik}{r}+\frac{3}{r^2}) + \hat{x}\hat{x}(-\frac{1}{r^2}-\frac{ik}{r}) \quad \text{(B.5)}$$

Yielding Equation B.6 for $\nabla\nabla g$

$$\nabla\nabla g = g(\hat{r}\hat{r}(-k^2+\frac{3ik}{r}+\frac{3}{r^2}) + I(-\frac{ik}{r}-\frac{1}{r^2}) \quad \text{(B.6)}$$

And finally from inserting Equation B.6 in the definition of G, Equation B.1, the identification used in the optical model yields.

$$G = (\frac{1}{k^2}\nabla\nabla g + Ig) = [I(1-\frac{i}{rk}-\frac{1}{(rk)^2}) - \hat{r}\hat{r}(1-\frac{3i}{rk}-\frac{3}{(rk)^2})]g(r) \quad \text{(B.7)}$$

B.2 The derivation of Gg

The Taylor series of 3^{rd} degree is taken for g(r). This is a good approximation of g(r) for small r.

$$g(r) = \frac{e^{-ikr}}{4\pi r} \approx \frac{1-ikr-\frac{1}{2}(kr)^2+\frac{i}{6}(kr)^3}{4\pi r} \quad \text{(B.8)}$$

The expression for G from Appendix B.1 is used.

$$G = [I(1-\frac{i}{kr}-\frac{1}{(kr)^2}) - \hat{r}\hat{r}(1-\frac{3i}{kr}-\frac{3}{(kr)^2})]g(r), r \neq 0 \quad \text{(B.9)}$$

Equation B.8 and Equation B.9 is now inserted in $G \cdot g$:

$$G \approx [I(1-\frac{i}{kr}-\frac{1}{(kr)^2}) - \hat{r}\hat{r}(1-\frac{3i}{kr}-\frac{3}{(kr)^2})][\frac{1-ikr-\frac{1}{2!}(kr)^2+\frac{i}{3!}(kr)^3}{4\pi r}] \quad \text{(B.10)}$$

For simplicity this step is broken in two. At first the terms with the factor, I is considered.

$$
\begin{aligned}
&= I[1 - \frac{i}{kr} - \frac{1}{(kr)^2}]g(r) \\
&= I[1 - ikr - \frac{1}{2}(kr)^2 + \frac{i}{6}(kr)^3 - \frac{i}{kr} - 1 + \frac{i}{2}kr + \frac{1}{6}(kr)^2 - \frac{1}{(kr)^2} + \frac{i}{kr} + \frac{1}{2} - \frac{i}{6}kr] \\
&= I[\frac{1}{2} - ikr + \frac{1}{2}ikr - \frac{1}{6}ikr - \frac{1}{2}(kr)^2 + \frac{1}{6}(kr)^2 + \frac{i}{6}(kr)^3 - \frac{1}{(kr)^2}] \\
&= I[\frac{1}{2} - \frac{2}{3}ikr - \frac{1}{3}(kr)^2 + \frac{i}{6}(kr)^3 - \frac{1}{(kr)^2}]
\end{aligned}
$$

As this is an approximation the last modification is made under the assumption that r is very small, so that terms containing r or r^2 is set to zero.

The second term of Equation B.10 is now evaluated.

$$
\begin{aligned}
&= \hat{r}\hat{r}(1 - \frac{3i}{kr} - \frac{3}{(kr)^2})g(r) \\
&= \hat{r}\hat{r}[1 - ikr - \frac{1}{2}(kr)^2 + \frac{i}{6}(kr)^3 - \frac{3i}{kr} - 3 + \frac{3}{2}ikr + \frac{1}{2}(kr)^2 - \frac{3}{(kr)^2} + \frac{3i}{kr} + \frac{3}{2} - \frac{i}{2}kr] \\
&= \hat{r}\hat{r}[-\frac{1}{2} - ikr + \frac{3}{2}ikr - \frac{1}{2} + \frac{i}{6}(kr)^3 - \frac{3}{(kr)^2}] \\
&= \hat{r}\hat{r}[-\frac{1}{2} + \frac{i}{6}(kr)^3 - \frac{3}{(kr)^2}]
\end{aligned}
$$

Due to the fact that r is very small it can be seen that term will be dominated by the last part of it and since this is an approximation the two other parts can be set to zero. The final expression of $Gg(r)$ is therefore:

$$
G \approx \frac{1}{4\pi r}(I[-\frac{2}{3}ikr - \frac{1}{(kr)^2}] - \hat{r}\hat{r}[-\frac{3}{(kr)^2}]) = \frac{1}{4\pi k^2 r^3}(-I + 3\hat{r}\hat{r}) - i\frac{k}{4\pi}I \tag{B.11}
$$

B.3 definitions in spherical coordinates

The definition of the unity dyad in spherical coordinates is given by Equation B.12.

$$
I = \hat{r}\hat{r} + \hat{\theta}\hat{\theta} + \hat{\phi}\hat{\phi} \tag{B.12}
$$

The three unit vectors in the spherical unity dyad are $\hat{r}$, $\hat{\theta}$, and $\hat{\phi}$. $\hat{r}$ is a unit vector in the direction of r, $\hat{\phi}$ is in the x,y plane of cartesian coordinates

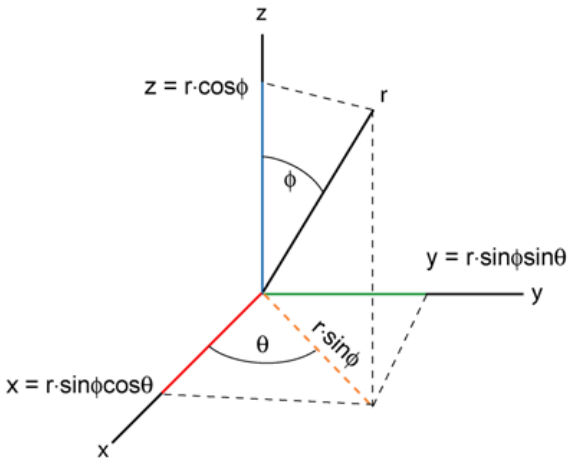

Figure B.1: Spherical coordinates

and is perpendicular to projection of the r vector into the x,y plane. $\hat{\theta}$ is in the $\mathbf{r}, \hat{z}$ plane and is perpendicular to the $\mathbf{r}$ vector.

Og det giver for:

$$\hat{z} \cdot I = \hat{r}(\hat{z} \cdot \hat{r}) + \hat{\theta}(\hat{z} \cdot \hat{\theta}) + \hat{\phi}(\hat{z} \cdot \hat{\phi}) = \hat{r}\cos\theta + \hat{\theta}\cos(\theta + \frac{\pi}{2}) + 0 = \hat{r}\cos\theta + \hat{\theta}\sin\theta \tag{B.13}$$

B.4 An approximation of the Dielectric Constant

Appendix C

Calculations for the optical model